



# Deciphering the contrasting climatic trends between the central Himalaya and Karakoram with 36 years of WRF simulations

Jesse Norris<sup>1,3</sup> · Leila M. V. Carvalho<sup>1,2</sup> · Charles Jones<sup>1,2</sup> · Forest Cannon<sup>1,2,4</sup>

Received: 24 May 2017 / Accepted: 29 January 2018 / Published online: 22 February 2018  
© Springer-Verlag GmbH Germany, part of Springer Nature 2018

## Abstract

Glaciers over the central Himalaya have retreated at particularly rapid rates in recent decades, while glacier mass in the Karakoram appears stable. To address the meteorological factors associated with this contrast, 36 years of Climate Forecast System Reanalyses (CFSR) are dynamically downscaled from 1979 to 2015 with the Weather Research and Forecasting (WRF) model over High Mountain Asia at convection permitting grid spacing (6.7 km). In all seasons, CFSR shows an anti-cyclonic warming trend over the majority of High Mountain Asia, but distinctive differences are observed between the central Himalaya and Karakoram in winter and summer. In winter and summer, the central Himalaya has been under the influence of an anti-cyclonic trend, which in summer the downscaling shows has reduced cloud cover, leading to significant warming and reduced snowfall in recent years. Contrastingly, the Karakoram has been near the boundary between large-scale cyclonic and anti-cyclonic trends and has not experienced significant snowfall or temperature changes in winter or summer, despite significant trends in summer of increasing cloud cover and decreasing shortwave radiation. This downscaling does not identify any trends over glaciers in closer neighboring regions to the Karakoram (e.g., Hindu Kush and the western Himalaya) where glaciers have retreated as over the central Himalaya, indicating that there are other factors driving glacier mass balance that this downscaling is unable to capture. While this study does not fully explain the Karakoram anomaly, the identified trends detail important meteorological contributions to the observed differences between central Himalaya and Karakoram glacier evolution in recent decades.

## 1 Introduction

Accelerated melting of alpine glaciers provides compelling evidence of the changes in the climate system caused by global warming. However, while most glaciers have generally retreated in recent decades, in some cases increasing glacier melt may be offset by regional snowfall and/or temperature trends. This intriguing behavior seems particularly

evident over High Mountain Asia, where significant differences between glacier mass balances have been observed (Hewitt 2005; Scherler et al. 2011; Bolch et al. 2012; Kaab et al. 2012). Specifically, glaciers in the central Himalaya exhibit some of the fastest retreat rates on Earth, while many glaciers in the Karakoram appear to be stable or advancing (Scherler et al. 2011; Bolch et al. 2012; Gardelle et al. 2012; locations of glaciers shown in Fig. 1). Glaciers function as reservoirs of moisture from precipitation, and regional populations and ecosystems depend on water resources provided by their meltwater during summer months (Hewitt 2005). Therefore, predicting future water resources requires an understanding of how changes in atmospheric circulation and thermodynamics have contributed to the evolution of glaciers in recent decades, and whether these changes will remain, cease, or intensify in future years as the planet warms.

Distinct seasonal precipitation regimes are observed over High Mountain Asia (Bookhagen and Burbank 2010). While precipitation over central Himalaya is almost solely dependent on summer precipitation, precipitation over the

---

✉ Jesse Norris  
jessenorris@ucla.edu

<sup>1</sup> Earth Research Institute, University of California Santa Barbara, Santa Barbara, CA 93106, USA

<sup>2</sup> Department of Geography, University of California Santa Barbara, Santa Barbara, CA 93106, USA

<sup>3</sup> Present Address: Atmospheric and Oceanic Sciences, University of California Los Angeles, Los Angeles, CA 90095, USA

<sup>4</sup> Present Address: Scripps Institution of Oceanography, University of California San Diego, San Diego 92093, CA, USA

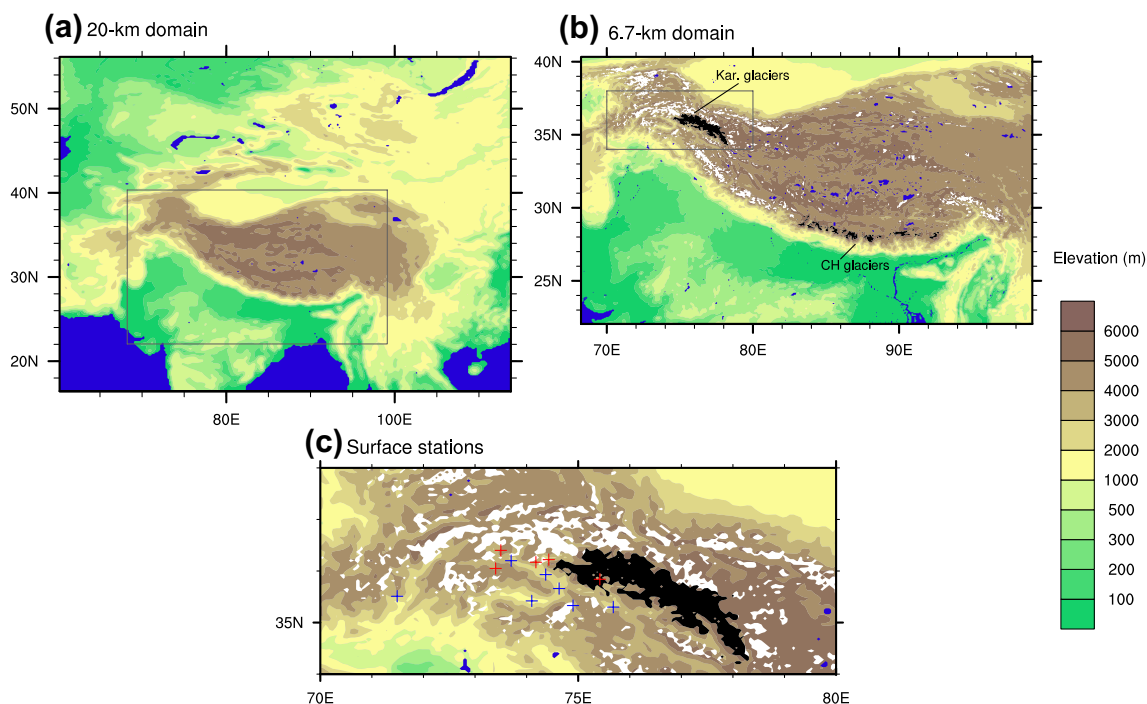


**Fig. 1** **a** The outer domain; **b** the inner domain; and **c** a zoomed-in portion of the inner domain showing the locations of the WAPDA (red) and PMD (blue) stations. All panels show elevation (colors) and water bodies (blue). The inner domain also shows glacier outlines

interpolated onto the WRF domain (white), highlighting those in the central Himalaya and Karakoram (black). The boxes in the first two panels indicate the area plotted in the subsequent panel

Karakoram is more evenly distributed through the year, with the greatest contributions in winter and spring from extratropical cyclones, which are also known as the winter westerly disturbances (e.g., Lang and Barros 2004; Barros et al. 2006; Cannon et al. 2015; Norris et al. 2015). Hence, changes to the summer monsoon system would be expected to have more of an effect on central Himalayan glaciers, while changes to winter westerly disturbances would more directly affect Karakoram glaciers. However, climatologically, both regions experience the greatest temperatures and hence the most degree days in summer. Degree days are the above-zero near-surface temperature integrated over time and taken as a proxy for the available energy for glacier melt (e.g., Rango and Martinec 1995). Given the large contribution of summer warming to glacier melt in both regions, summertime changes in weather patterns, precipitation and cloudiness are equally relevant for both regions in terms of glacier melt.

The rapid retreat of central Himalayan glaciers has been attributed to increasing summer temperatures at high elevations (Yamada et al. 1992; Shrestha et al. 1999; Hasnain 2002). Changes to the South Asian summer monsoon precipitation, however, are particularly relevant for central Himalayan glaciers, given that a large majority of precipitation over this region falls in summer (e.g., Bookhagen and Burbank 2010). Many studies have found that precipitation

associated with the South Asian summer monsoon has decreased over the 20th Century, due to greater warming of the Indian Ocean than the land, hence a dynamical weakening of the monsoon (e.g., Krishnan et al. 2013; Zhao et al. 2014; Roxy et al. 2015). Although large-scale decreases in monsoon precipitation do not necessarily imply a decrease over the Himalaya, Duan et al. (2006) analyzed ice cores from a central-Himalayan glacier and suggested significant decreases in orographic monsoon precipitation during the twentieth century. Therefore, the evidence suggests that increasing temperatures and decreasing precipitation in summer have both been contributing to glacier retreat over the central Himalaya.

Contrastingly, the advance of some glaciers over the Karakoram has been attributed to increasing precipitation in winter and summer (Archer and Fowler 2004), as well as decreasing summer temperature (Fowler and Archer 2006; Forsythe et al. 2017). Consistent with increasing (decreasing) winter precipitation over the Karakoram (central Himalaya), Cannon et al. (2015) identified an increase in the frequency and intensity of upper-level troughs affecting the Karakoram from 1979 to 2010, together with a corresponding decrease in troughs affecting the central Himalaya. Forsythe et al. (2017) quantified the large-scale circulation over southwest Asia by defining the Karakoram Zonal Index (KZI), which is positive (negative) when there is an

anti-cyclonic (cyclonic) anomaly. They showed a significant negative trend in the KZI over recent decades in summer months and showed a significant correlation with a cooling trend in the upper Indus basin, near the Karakoram. They attributed the cooling to adiabatic cooling due to the vertical circulation associated with the cyclonic trend, increased cloudiness, and decreased insolation. Contrastingly, the central Himalaya is more under the influence of a vortex over the subcontinent associated with the monsoon that is anomalously anti-cyclonic when the KZI is anomalously cyclonic. Therefore, although only a few hundred km apart, the Karakoram and central Himalayan glaciers appear to have been under the influence of contrasting climatic trends in both winter and summer over the last few decades.

It is important to note that examining trends in precipitation and temperature in this region is challenging for many reasons. Difficulties include limited in-situ measurements and bias toward sampling at low-elevation sites, which are more accessible but may be unsuitable proxies for high elevations due to significant orographic gradients (e.g., Barros and Lang 2003; Norris et al. 2017). Although a few in-situ measurements have exhibited likely precipitation and temperature trends over the central Himalaya and Karakoram (e.g. Archer and Fowler 2004), the uneven distribution of these data over High Mountain Asia (Bookhagen and Burbank 2010) restricts the analysis of the spatial patterns of these trends. Also, station precipitation measurements are prone to large errors at exposed high elevations (Bollasina et al. 2002; Tahir et al. 2011). Furthermore, different datasets span different time periods, and there are very few that date back to the beginning of the period during which the contrast between glacier retreat/advance over the central Himalaya and Karakoram has been observed (roughly 1980 to the present). Ideally, datasets covering the full region at high spatial resolution and dating back to 1980 are required to adequately represent the spatiotemporal patterns of temperature and precipitation in High Mountain Asia. Additionally, atmospheric data at high temporal and spatial resolution are necessary to understand mechanisms whereby synoptic-scale systems interact with topography and how these interactions may further influence glacier mass balance.

Although global reanalyses can be useful to describe variations and changes to large-scale flow patterns over south Asia in recent decades, their coarse resolutions poorly represent the complex topography of the Himalaya and Karakoram and, consequently, the interactions of synoptic-scale weather systems with the steep terrain (Cannon et al. 2017; Norris et al. 2015, 2017). With the goal of investigating historical climate change over the Tibetan Plateau, Gao et al. (2015) performed 32 years (1979–2011) of downscaling simulations of the Interim European Centre for Medium-Range Weather Forecasts (ECMWF) Re-Analysis (ERA-Interim, Dee et al. 2011) using the Weather Research and

Forecasting (WRF) model at 30-km grid spacing. While the downscaling at 30-km grid spacing improved existing reanalyses in describing large-scale climatic patterns, 30 km is still somewhat coarse in terms of resolving orographic precipitation patterns, particularly in summer. The importance of resolution for representing summer flow patterns over the Himalaya was illustrated by Norris et al. (2017). In particular, 10-km simulations with parameterized convection do not capture the significant nocturnal precipitation that falls over the Himalaya in summer, whereas 6.7-km simulations without convective parameterization simulate a diurnal cycle similar to station measurements, and no fundamental improvement is made by decreasing to 2-km grid spacing (Norris et al. 2017). This nocturnal summer precipitation has been well documented (e.g., Barros and Lang 2003; Houze et al. 2007; Medina et al. 2010), and according to the station measurements constitutes the majority of summer precipitation (Fig. 13 of Norris et al. 2017), hence must be represented by a dataset in order to diagnose trends in these areas.

The main objective of this study is to assess the spatial pattern of precipitation (in particular, snowfall) and temperature trends in High Asia and decipher the underlying physical and dynamical atmospheric mechanisms responsible for the observed contrasting trends between the western and central Himalaya's climate in recent decades. Specifically, this study investigates changes in circulation and geopotential patterns and how these changes modified orographic snowfall and cloudiness that ultimately resulted in the observed contrasting climatic trends between the central Himalaya and the Karakoram. To capture the spatial distribution of orographic snowfall and temperature trends, this study uses WRF model at convection permitting grid spacing (6.7 km) to dynamically downscale 36 years (1979–2015) of global reanalyses over High Mountain Asia. The resulting model dataset describes the interannual and inter-decadal variability of all meteorological variables over the region in all seasons.

## 2 Data and methodology

### 2.1 Model configuration

The Advanced Research Weather Research and Forecasting (WRF) model version 3.7.1 (Skamarock et al. 2008) was used to dynamically downscale 36 full years of Climate Forecast System Reanalysis (CFSR, Saha et al. 2010), which is at 0.5° grid spacing, from April 1979 through March 2015 over High Mountain Asia. Each year was simulated exactly as the single year simulated in Norris et al. (2017) (hereafter N16). Specifically, the model was initialized at 00 UTC 1 March each year and run continuously until 00 UTC 1 April the following year, with the initial March output

discarded as model spin up, hence 12 months of retained output. Although 1-month spin up may not be sufficient for optimal accuracy, particularly with land-surface processes, according to N16 it is an acceptable tradeoff considering the computational demand of high-resolution multi-decadal downscaling. Crucially though, each year of output is generated in exactly the same way, so that interannual variability and trends may be investigated. Each year of model data spans April through March, as opposed to a full calendar year, so that each year contains one full monsoon and winter season. Therefore, when calculating trends for given seasons (see Sect. 2.2), each year of output can be used as one entry in a 36-entry time-series.

The justification for using CFSR over this region, as opposed to other reanalyses, was given in N16. CFSR and ERA-Interim are the best performing reanalyses over the Tibetan Plateau (Bao and Zhang 2013). Therefore, provided that the reanalysis is consistent during the downscaling period, trend analyses from the downscaling are reliable. Importantly, we show that the trends in the large-scale flow patterns shown by CFSR, which are downscaled by WRF in this study, are in agreement with those derived from ERA-interim (discussed in Sect. 3).

Two nested domains of 20- and 6.7-km grid spacing were configured for the WRF downscaling (Fig. 1) with 50 model levels from the surface up to 50 hPa. Although about 2-km or smaller grid spacing is generally considered necessary to represent orographic precipitation and explicitly resolve convection, N16 showed that 6.7 km grid spacing was sufficient for simulating both winter and summer precipitation patterns over the Himalaya and Karakoram, and that a 2.2-km domain did not capture any fundamentally different spatiotemporal precipitation patterns, including the diurnal cycle. Crucially, 6.7 km is just small enough that convective parameterization may be switched off, as shown by N16—the same study demonstrated that explicit treatment of convection is necessary to capture diurnal cycles over the Himalaya. Although smaller grid spacing would undoubtedly capture some finer-scale variability in trends than is exhibited by the 6.7-km downscaling, 6.7 km is considered an acceptable tradeoff, given the computational demand of simulating 36 years. The model output was saved every 3 h, so that weather patterns at all times of day were represented. Spectral nudging (Stauffer and Seaman 1990; Stauffer et al. 1991) of zonal and meridional wavenumbers 1–5 and 1–4, respectively, was applied to temperature, winds, and geopotential height in the outer domain and all vertical levels, described in more detail in N16. This nudging implies that the downscaling responds indirectly to external forcing of the climate (e.g., increased greenhouse gas concentrations) via temperature increases in the reanalyses.

The parameterizations used were justified in N16 and are as follows: Thompson microphysics (Thompson et al. 2008);

Yonsei University boundary layer (Hong et al. 2006); MM5 Monin–Obukhov surface layer (Monin and Obukhov 1954); Noah-MP land surface (Niu et al. 2011); RRTMG longwave and shortwave radiation (Iacono et al. 2008); Kain–Fritsch convection (Kain 2004, outer domain only). For seasonal simulations over complex terrain, cloud cover and precipitation are most sensitive to the choice of microphysics scheme, with Thompson among the best performing (Liu et al. 2011). Importantly, the radiation and microphysics schemes interact, and in particular the RRTMG scheme uses cloud water, cloud ice, and snow when calculating radiative fluxes, which performs well when coupled with Thompson microphysics (Thompson et al. 2016). Although this coupling does not consider droplet sizes when calculating radiative fluxes, the simple relationship of greater cloud cover or hydrometeors (in terms of mixing ratio) equals less radiation at the surface and, therefore, less surface warming can be simulated. As will be shown, this relationship is critical to the current study. Although biases exist in the parameterization schemes utilized in this downscaling, if these biases are approximately consistent with time, then the downscaling may be used to diagnose trends in cloud, radiation, and snowfall during the downscaling period.

## 2.2 Trend analysis

For each year of model output, the total or mean value of a given variable over a season (MAM, JJA, SON, and DJF) was calculated at each grid point. Thus, for a given variable, season, and grid point, a time series of 36 values represented the interannual variability and trend from 1979–2014 (where 1979 means April 1979 through March 1980 and likewise for other years). For 3-D variables, output was first interpolated onto pressure levels and then a separate time series generated at each level. Trend analysis was performed on these 36-element time series using a two-tailed Monte Carlo significance test (Wilks 2006). The Monte Carlo test assesses whether the elements of a time series are ordered in a significantly upward or downward trend. The given time series is taken and its elements shuffled into a random order  $N$  times (10,000 in the current study), with the magnitude of the trend for each shuffled time series recorded. The  $p$  value is then the fraction of the  $N$  trials whose trend is of a greater magnitude than that of the original time series. This approach led to 2-D and 3-D arrays of the trend and significance level of each time series, which are visualized throughout this study via horizontal maps and cross sections. Trends were also calculated with the Mann–Kendall significance test (Wilks 2006), with no meaningful change in the results.

Trend analysis was also performed with the same Monte Carlo test by taking the spatial average of a given variable over the central Himalaya (hereafter, CH) and Karakoram

glaciers. The areas covered by the CH and Karakoram glaciers are shown in Fig. 1b. These areas are where the Randolph Glacier Inventory 5.0 (<http://www.glims.org/RGI/>) has been bilinearly interpolated onto the 6.7-km WRF domain. Each grid point in the Randolph Glacier Inventory is either 1 or 0 for glacier cover or no glacier cover, and WRF grid points are considered glaciated if the interpolated value is greater than 0.5. The full extent of glacier coverage over the 6.7-km domain is shown in white, but those that lie within the CH and Karakoram are shown in black. Specific glaciated grid points that qualify as CH and Karakoram have been determined manually for this study. Some trends are calculated at 500 hPa which is below the surface of some CH and Karakoram grid points and so these grid points were excluded from the CH or Karakoram average in those instances.

### 2.3 In-situ measurements

In-situ measurements in the upper Indus basin are used to evaluate the precipitation and temperature trends shown by the WRF downscaling over the Karakoram. Although this study investigates simulated snowfall trends, total-precipitation trends from WRF are used for comparison to station data because the stations do not distinguish between rain and snow. Interannual time series were constructed using the mean of seven stations operated by the Pakistan Meteorological Department (PMD) ranging from 1250 to 2210 m (marked in blue in Fig. 1c—see Table 2 of N16 for the individual stations names and elevations). These stations' data period extends from 1960 to 2012, so almost the full period of the downscaling could be compared between WRF and the stations. However, although near the Karakoram, these stations are considerably lower than the elevations of the glaciers, which are between 4000 and 5500 m on the WRF grid. In winter, precipitation in the Indus valley is generally highly correlated with that over the Karakoram (N16), but in summer this is not a reasonable assumption as mechanisms generating precipitation are more complex and differ between valleys and peaks. Therefore, in addition to comparisons with the PMD stations, time series were constructed from the mean of five stations operated by the Pakistan Water and Power Development Authority (WAPDA) at higher elevations (2898–4440 m, marked in red in Fig. 1c—see Table 2 of N16). These data are only available from 1995 through 2009. Although these stations likely underestimate precipitation by a high factor (Tahir et al. 2011) as suggested by comparisons with WRF in N16, trends may be realistic if the negative bias remains fairly consistent over the years, as is investigated in Sect. 4.1. For both the PMD and WAPDA stations, there are some missing data over the respective time periods for certain stations, and so the mean time series is calculated by calculating the daily

mean values from whichever stations have available data on the given day, and then aggregating to mean (temperature) or total (precipitation) over the given season. Years when a significant number of stations had missing data for large parts of winter/summer impacted the comparisons with WRF, as will be discussed.

Station data over the central Himalaya were also sought to exhibit trends consistent with glacier retreat observed over the central Himalaya in recent decades. However, excessive data gaps and discontinued station records prevented the identification of any significant trends during the period simulated. APHRODITE (Yasutomi et al. 2011; Yatagai et al. 2012) which gives gridded precipitation and temperature estimates over recent decades, based on interpolated station measurements, was also analyzed, but did not yield a coherent spatial distribution of trends over the Himalaya or Karakoram, likely due to poor representation of stations over those ranges.

### 2.4 MODIS cloud cover

Cloud cover from the Moderate Resolution Imaging Spectroradiometer (MODIS) Cloud Product (MOD06L2) at 5-km grid spacing was used to evaluate the interannual variability of cloud cover over High Asia shown by WRF. This product is obtained by combining visible and infrared images from two daily satellite passes at about 0900 and 2100 local time, indicating whether or not cloud was present at a given pixel during a given pass. To compare these data with WRF, first the MODIS data was interpolated onto the WRF grid, then at each grid point and for each winter and summer the mean cloud fraction was calculated, i.e., the fraction of times over the given winter or summer on which there was cloud cover. For WRF, the cloud fraction was set to 1 if there was cloud at any vertical level, based on the 3-D cloud fraction. The MODIS data period begins in July 2002, so 2002–2003 onward was used for winter and 2003 onward for summer. For MODIS, the mean was calculated of the two daily passes and over the given winter and summer, i.e., the mean of 180 cloud passes for DJF (182 for leap years) and 184 for JJA. For WRF, the mean was calculated over a given winter or summer taking just the 0300 and 1500 UTC values (roughly 0900 and 2100 local time, i.e., those closest to the times of the MODIS data). However, using all eight WRF output times per day made very little difference to the comparisons between WRF and MODIS. For both WRF and MODIS, a value was thus calculated for each winter and summer, and interannual time series constructed from these values, allowing for a comparison of the interannual variability of cloud cover between WRF and MODIS. Although the MODIS data period is not long enough to

diagnose trends, this dataset is useful to examine correlations with WRF over the available time period.

### 3 Changes in large-scale climatic patterns (1979–2015)

Deciphering the dynamical and physical mechanisms explaining the contrasting regional climatic trends in the central Himalaya and Karakoram requires a careful analysis of the recent changes in the large-scale flow patterns of south Asia and whether these alterations are seasonally dependent. We start this study by examining trends in 200-hPa geopotential height and winds using CFSR because these are the reanalyses that are downscaled by WRF. At 500-hPa, the trends are morphologically similar but less spatially coherent over High Asia because of elevation. Figure 2 illustrates the warming of the tropical troposphere of the Northern Hemisphere in recent decades and demonstrates consistent warming in all seasons.

However, in all seasons, cyclonic trends indicated by the wind vectors are co-located with gaps in the area of positive geopotential-height trends, although there are some gaps where the wind trends are not significant. Therefore, particularly in winter and summer, according to the reanalyses, the intensification of the cyclonic flow may have offset the warming west of High Asia resulting in a neutral trend in geopotential height.

In winter, the eastern part of High Asia is under the influence of a warming trend (High Asia is indicated by the 3-km elevation contour), whereas there is no statistically significant trend over the western part (Fig. 2a). However, a pronounced cyclonic trend is observed in Asia's extratropics and the southern flank of this trough is co-located with western High Asia. The patterns of winter trends in 200-hPa winds and geopotential height indicate an intensification of the warming in the subtropics east of High Asia. The winter trend does not resemble the climatology, so that the area with the cyclonic trend reflects a weakening of the ridge over northwestern Asia and the area with the anti-cyclonic trend

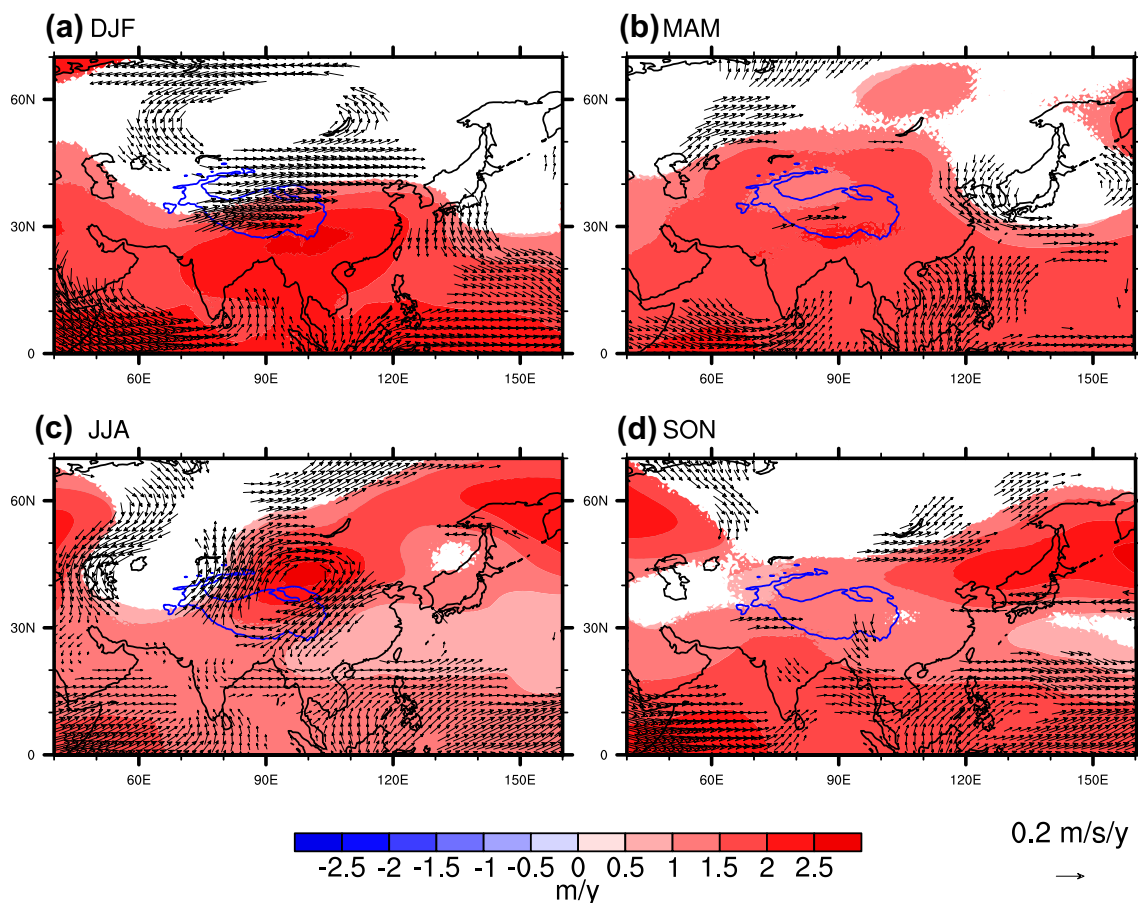


**Fig. 2** CFSR trends over Asia from 1979–1980 to 2014–2015 for each season individually. The trends shown are 200-hPa geopotential height (colors, m/year), only plotting trends that are significant at the

5% level, and wind vectors ( $\text{m s}^{-1}/\text{year}$ , plotted where either  $u$  or  $v$  has a trend that is significant at the 5% level. The 3-km elevation contour is plotted to indicate the location of High Asia

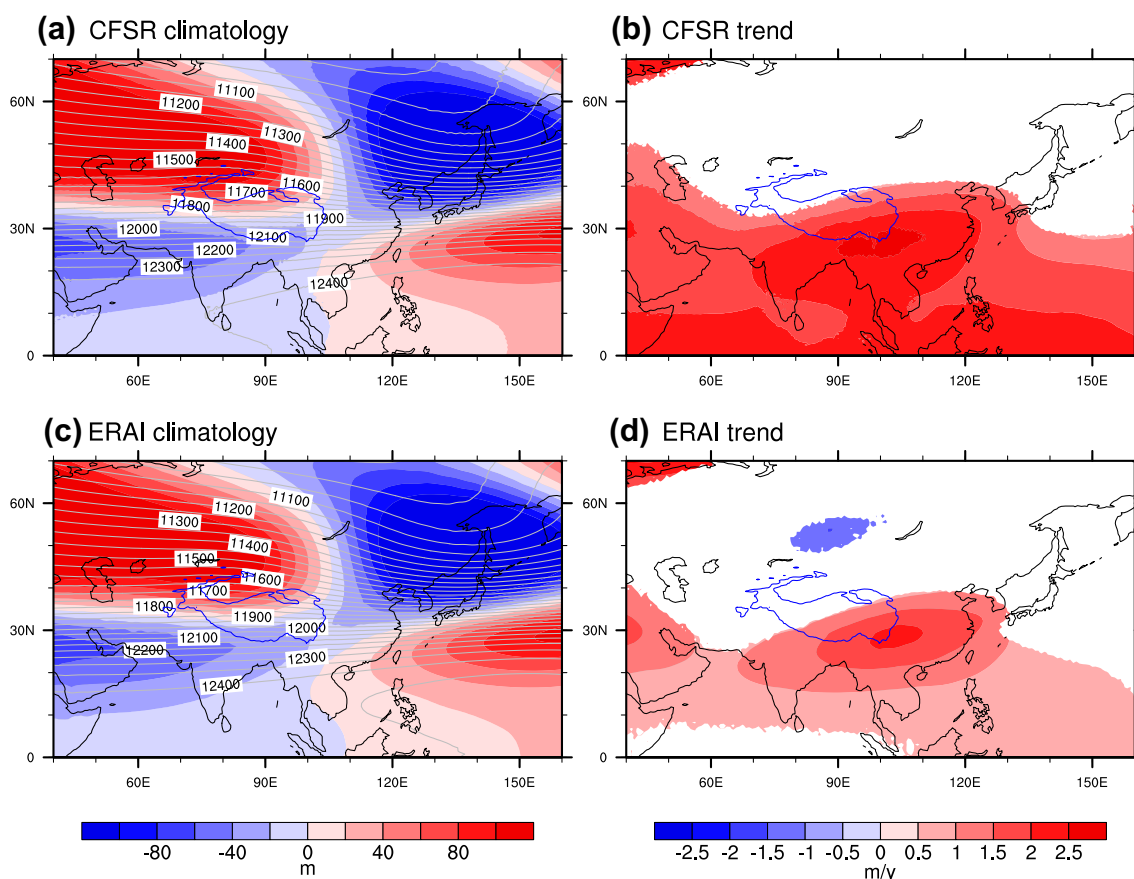


**Fig. 3** Comparisons of CFSR (top panels) and ERA-Interim (bottom panels), showing climatologies (left panels) and significant trends at the 5% level (right panels) in 200-hPa geopotential height in DJF from 1979–1980 to 2014–2015. Climatologies show abso-

lute values (labeled gray contours every 50 m), as well as the values obtained by removing the zonal mean of the area shown (colors, m). The 3-km elevation contour is also plotted

reflects a weakening of the trough over southeastern Asia (Fig. 3, top panels). These features are consistent with the increase (decrease) in the synoptic activity associated with the winter westerly disturbances affecting the Karakoram (central Himalaya) discussed in Cannon et al. (2015).

In summer, there is an anti-cyclonic trend in the 200-hPa flow north and east of High Asia accompanied by a cyclonic trend west of High Asia (Fig. 2c). This trend reflects a weakening of the climatological ridge over southwest Asia and of the troughs north and east of High Asia (Fig. 4, top panels). This pattern may be due to warming of the Tibetan Plateau at a greater rate than its surroundings and the location of the upper-tropospheric anti-cyclonic anomaly is similar to that of Wang et al. (2008, their Fig. 3c) in numerical experiments of Tibetan Plateau warming. However, Zhao et al. (2014) exhibited similar trends in summer from the National Centers for Environmental Prediction and the National Center for Environmental Research (NCEP–NCAR) reanalyses and related them to a weakening of the South Asian summer monsoon. Similarly, Forsythe et al. (2017) showed a

significantly decreasing trend in the KZI (defined in the introduction), i.e., a cyclonic trend over southwest Asia. Because the Karakoram Vortex, as defined in that study, is coupled with the South Asian monsoon in summer and is anomalously cyclonic when the monsoon is anomalously anti-cyclonic, this implies a weakening of the monsoon, as has been identified in other studies (e.g., Krishnan et al. 2013; Zhao et al. 2014; Roxy et al. 2015). The trend may also be interpreted as an increasing influence of midlatitude westerlies in summer (Mölg et al. 2017)—the upper-tropospheric cyclonic and anti-cyclonic anomalies over High Asia when the influence of midlatitude westerlies in summer is enhanced (Fig. 3a of Mölg et al. 2017) are highly similarly distributed to the trend in Fig. 2c, suggesting that the westerlies have had an increasing influence in summer during the period of the downscaling. Therefore, the evidence suggests that the cyclonic and anti-cyclonic trends in summer (Fig. 2c) are associated with both a weakening monsoon and an increased influence of westerlies. Whether the weakening monsoon is the root cause of this regional trend remains

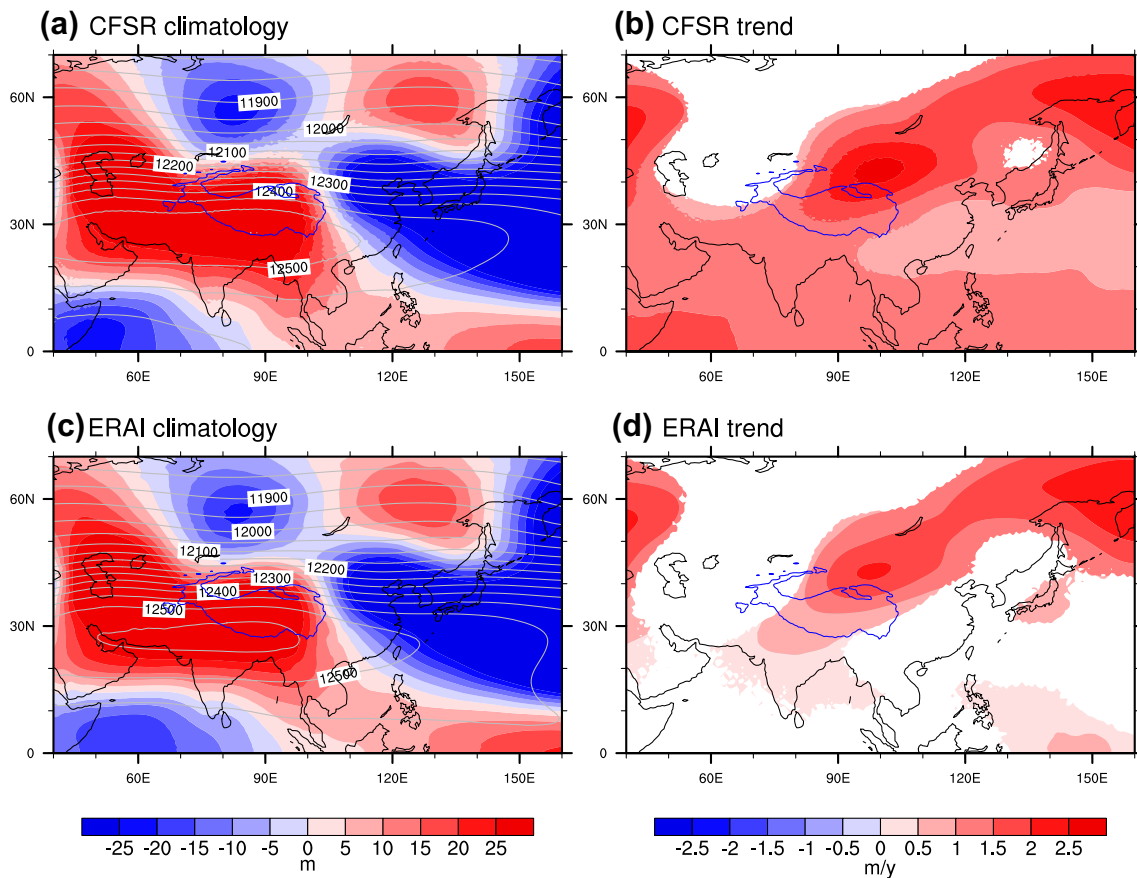


**Fig. 4** As Fig. 3, but for JJA from 1979 to 2014

an ongoing research question. Rather than with understanding the reasons for the atmospheric large-scale trends, the current study is concerned with their potential roles on the contrasting glacier behavior between the Karakoram and central Himalaya.

Because the WRF simulations performed for this study effectively downscale synoptic-scale features, it is important to establish that the CFSR trends are accurate. Therefore, the climatology and trend of 200-hPa geopotential height are compared between CFSR and ERA-Interim in winter (Fig. 3) and summer (Fig. 4). The climatology is almost identical between CFSR and ERA-Interim in both winter (Fig. 3, left panels) and summer (Fig. 4, left panels). Although the trend is similar between the two reanalyses, ERA-Interim shows the cyclonic trend extending farther south in both winter (Fig. 3, right panels) and summer (Fig. 4, right panels) and the positive geopotential-height trend is of lower magnitude than CFSR in both winter and summer. Crucially, CFSR and ERA-Interim agree that, in both winter and summer, most of High Asia, including the central Himalaya, has been under the influence of an anti-cyclonic trend, while the

northwestern part of High Asia, including the Karakoram, has not been affected by this trend.

The remainder of this paper is concerned with the effects of these large-scale trends in winter and summer on local snowfall and temperature according to the WRF downscaling. Before investigating the physical mechanisms associated with snowfall and temperature trends over the glaciers, the following section evaluates the interannual time series simulated by WRF over the glaciers using available in-situ and satellite data.

## 4 Evaluation of WRF with observations

### 4.1 In-situ measurements over and near the Karakoram

To evaluate the snowfall and temperature trends shown with WRF over the Karakoram region, this study compares the interannual time series of precipitation, daily-maximum 2-m temperature (T2m) and daily-minimum T2m for both winter and summer to those recorded by five WAPDA surface



stations near the Karakoram (Sect. 2.3). However, biases between observation and simulations are expected and have been discussed in N16. For precipitation, the magnitudes differ between the station and WRF, which N16 argued was most likely due to significant undercatch by the stations. For temperature, the magnitudes differ because the stations are lower than the mean elevation of all grid points that were utilized to construct the WRF time series. Nevertheless, assuming that measured and simulated errors are consistent through time, the time series may be compared to evaluate the ability of WRF to represent the interannual variability. Trends from WRF and the stations are plotted, and their significance levels indicated, but because the time period covered by the WAPDA stations is less than half the full time period of interest, these trends are in some cases not representative of the full 36 years.

In winter from 1995 to 2009, precipitation, maximum temperature, and minimum temperature are significantly correlated ( $p \leq 0.01$ ) between WRF and the stations at 0.70, 0.83, and 0.78, respectively (Fig. 5, left panels) and both WRF and the station measurements show a significant ( $p = 0.02$ ) increase in precipitation during this period (Fig. 5a). WRF and the stations also agree that there is almost no difference between maximum and minimum temperature in terms of interannual variability. In summer, correlations are lower (0.56, 0.52, and 0.55; Fig. 5, right panels), but significant at the 5% level, and the comparisons are impacted by missing station data. In particular, for the whole of JJA in 1997 (where there are large discrepancies between WRF and the stations for all variables), there are precipitation data for only one of the five WAPDA stations and temperature data for only two. Given the range in elevation between different stations, this implies a bias for that year when compared to other years. Excluding 1997, the precipitation correlation does not improve (0.55), but the correlations for maximum and minimum temperature increase to 0.87 and 0.89, respectively. The negative precipitation bias from the stations appears to be highly consistent through time, judging from the significant correlations between WRF and the stations for winter and summer (Fig. 5, top row). In particular, the greater discrepancy between WRF and the stations in winter than summer indicates that the stations do not effectively record snowfall.

To compensate for the relatively short record of WAPDA measurements in the time period of interest to this study, almost the full WRF time series over the Karakoram are compared to the mean of seven lower-elevation PMD stations in the upper Indus basin in Fig. 6. The average of precipitation records over a longer time period shows highly significant correlations with WRF for precipitation, maximum temperature, and minimum temperature in winter and summer. The station trends are

similar to those calculated by Forsythe et al. (2015), using three of the PMD stations and three of the WAPDA stations employed in this study, and the trends are generally consistent across stations in winter and summer (Forsythe et al. 2015, their Fig. 3). Unlike WRF, the stations show a significant ( $p = 0.04$ ) increasing trend in maximum winter temperature (Fig. 6b). However, this is not considered relevant to glacier melt because maximum winter temperature is still well below freezing at the elevation of the glaciers. The significant correlations of the WRF with station time series in Fig. 6 despite the climatological differences between the upper Indus basin and the Karakoram, combined with the significant correlations shown in Fig. 5 for the higher-elevation WAPDA stations, lends confidence to the trends exhibited by WRF over the Karakoram that are analyzed in this study. Crucially, there is agreement that the Karakoram/upper Indus basin has not been under the influence of any trends suggestive of glacier retreat, and so the observations and simulations are both consistent with the stable/advancing glaciers over the Karakoram.

#### 4.2 MODIS cloud cover over the Himalaya and Karakoram

The motivation of this section is to establish how accurate WRF is in distinguishing cloudy years from less cloudy years. This issue is investigated by calculating correlations between WRF and MODIS cloud cover in terms of interannual variability. In summer, the correlation from 2003 to 2012 is above 0.5 over most of High Asia (Fig. 7b). In winter, the area of high correlation is smaller and does not include the CH (Fig. 7a).

When averaged over the Karakoram and CH during winter and summer, the cloud fraction from WRF is about double that of MODIS (Fig. 8). This is not surprising since the Thompson microphysics scheme has been found to substantially overestimate cloud ice in cloud-permitting simulations at similar grid spacing (Wang et al. 2009). This is relevant because cloud ice constitutes almost all winter cloud over these high elevations and even a great deal of summer cloud. The same study also found biases in the timing and duration of cloud formation using the Thompson scheme. However, assuming that the biases are fairly consistent, the most important comparison between WRF and MODIS for the current study is the interannual correlation. Winter cloud cover shows a correlation of 0.57 and 0.23 over the Karakoram and CH, respectively, and with  $p < 0.05$  for the Karakoram comparison (Fig. 8, top row). The low correlation for winter cloud cover over the CH is of little relevance since almost all precipitation falls during summer (not shown). Worth noticing, however, the

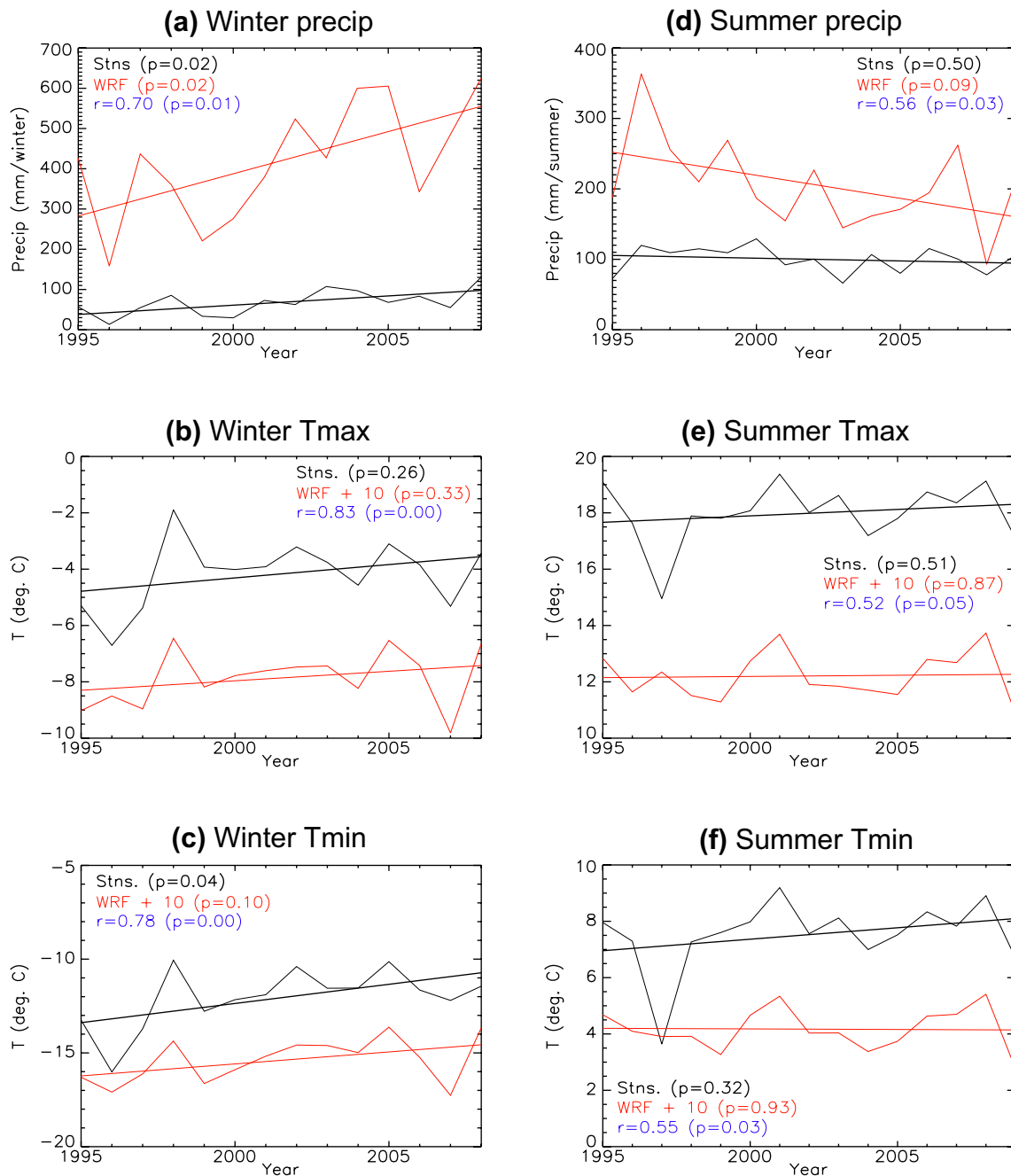


**Fig. 5** Time series comparisons between WRF and the mean of 5 WAPDA surface stations for precipitation, daily-maximum temperature, and daily minimum temperature in DJF (left panels) and JJA (right panels). The WRF panels are from the mean of all Karakoram grid points (shown in Fig. 1b). 10 °C is added to WRF temperature (since the WRF grid points are higher than the stations) in order to

plot the WRF and station time series together. The least-squares trend is also plotted for each timeseries and significance levels are indicated for each trend. Pearson correlations are given between the WRF and station timeseries in each panel, along with the significance of each correlation. Correlations and significance levels are rounded to two decimal places

WRF and MODIS time series are in fact very highly correlated except from 2010–2012 when WRF shows unusually cloudy years and MODIS does not (Fig. 8b). These years appear particularly cloudy in WRF due to the general lack

of cloud cover in winter over the CH, so that a small number of extreme events in one winter may double or even triple the mean number of cloudy days. In summer, the correlations are 0.66 and 0.50 over the Karakoram and CH,

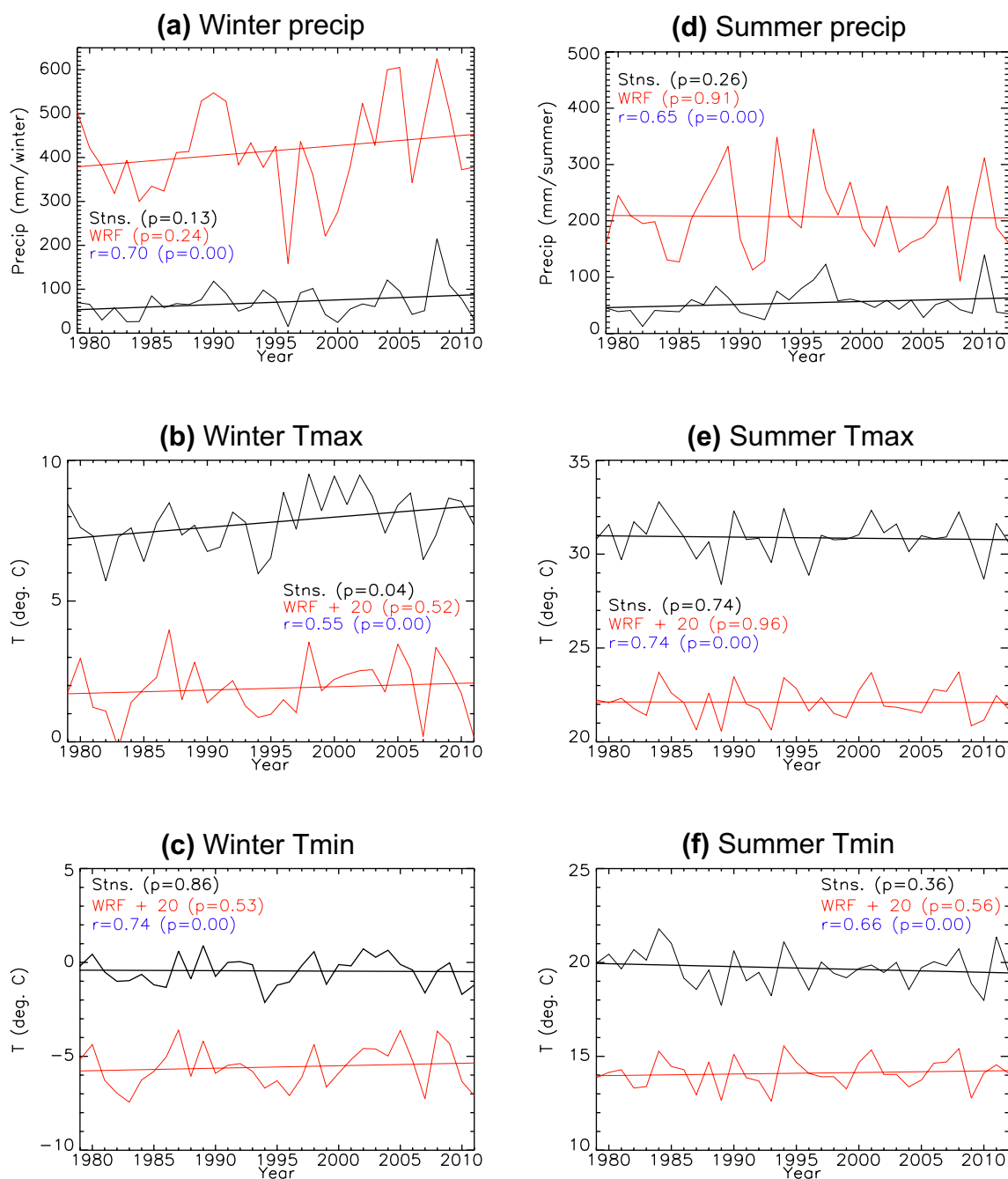


**Fig. 6** As Fig. 5, but over the longer time period and taking the mean of the 7 PMD stations. 20 °C is added to WRF temperature, since there is an even greater elevation difference between the WRF grid

respectively, and with  $p < 0.05$  for the Karakoram comparison (Fig. 8, bottom row). Although the comparisons between the WRF and MODIS time series are not perfect, agreement of interannual variability lends confidence to the trends in cloud cover exhibited by WRF and analyzed in the following section.

points and the stations than in Fig. 5, in order to plot the WRF and station time series together

## 5 Physical and dynamical mechanisms explaining regional trends

The objective of this section is to examine physical and dynamical mechanisms responsible for the trends in snowfall and T2m exhibited by WRF and how they vary according to the winter and summer seasons.

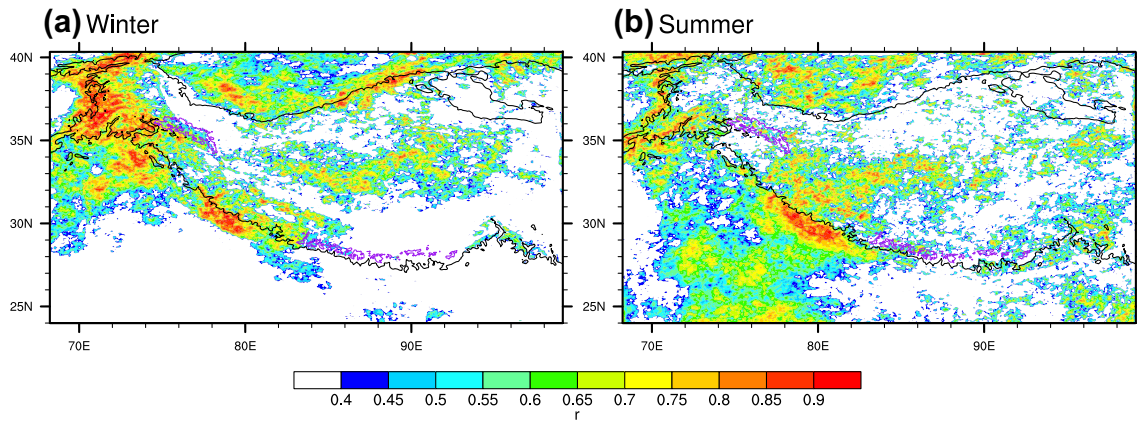


**Fig. 7** Correlation between WRF and MODIS of the interannual variability of cloud cover in DJF (from 2002–2003 to 2014–2015) and JJA (from 2003 to 2014). The 3-km elevation contour is plotted in black and the CH and Karakoram glacier outlines are purple

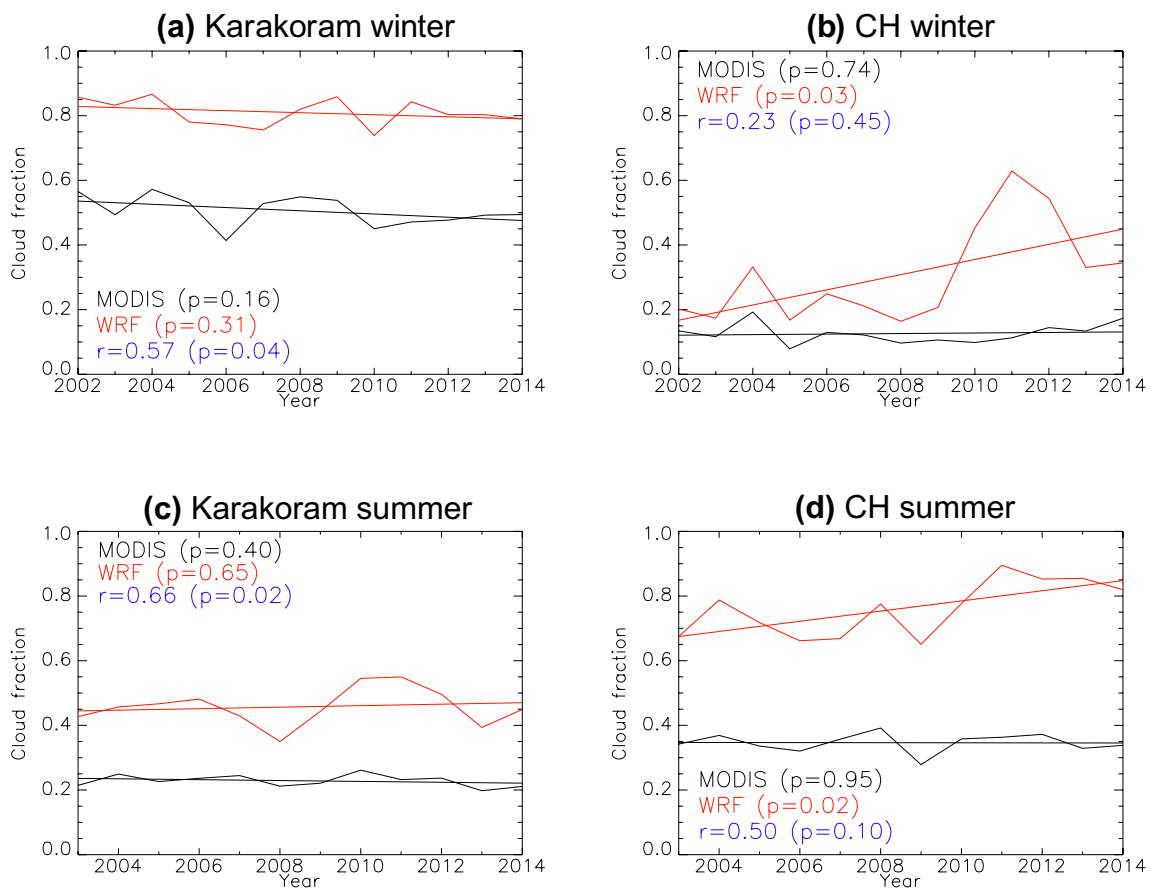


**Fig. 8** Interannual timeseries of mean cloud fraction from WRF and MODIS, averaging over the Karakoram (left panels) and CH (right panels) in DJF (top panels) and JJA (bottom panels). Trends are plot-

ted and their significances indicated, as in Figs. 5 and 6. Correlations are given, along with the significance of each correlation, as in Figs. 5 and 6

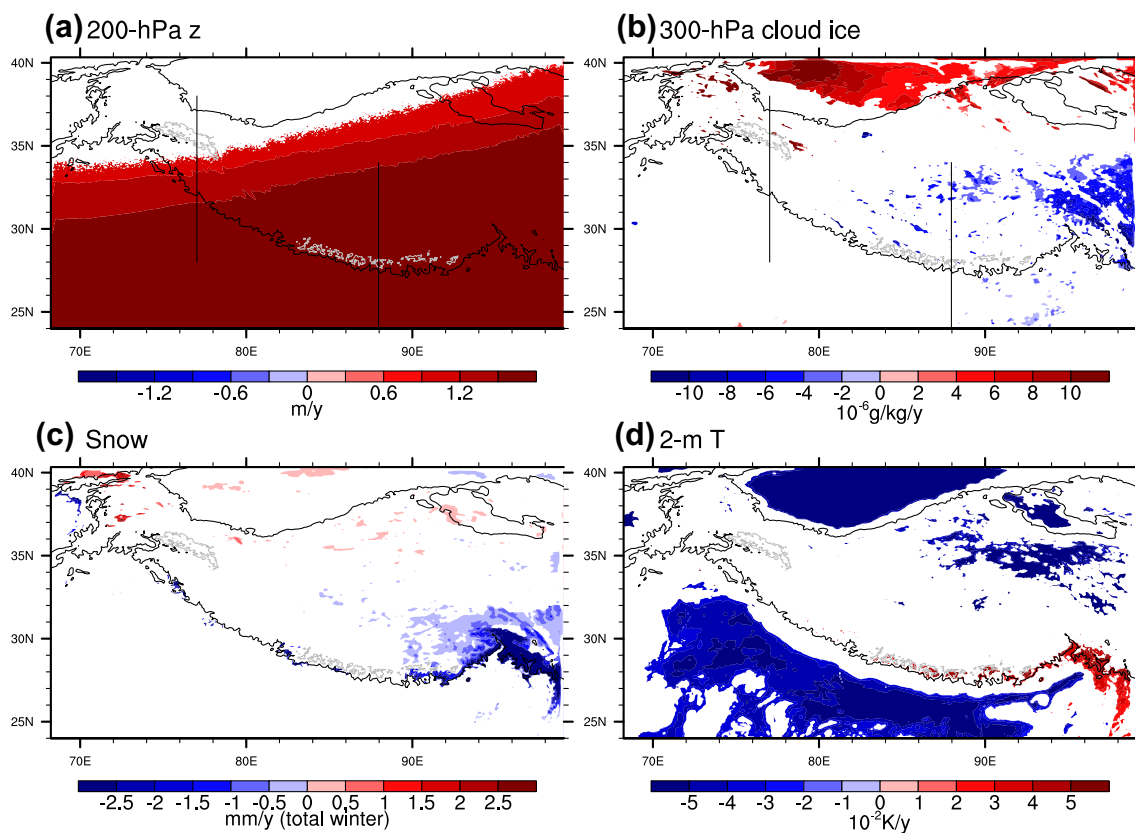


**Fig. 9** Trends of the given variables in DJF from 1979–1980 to 2014–2015, only plotted where the trends are significant at the 5% level. Also plotted are the 3-km elevation contour in black, and the CH and

Karakoram glacier outlines in gray. The lines in the panels of pressure-level variables show the locations of the cross sections across the western Himalaya/Karakoram and CH/Tibet in Fig. 10

## 5.1 Winter trends

### 5.1.1 Large-scale trends

In winter, the relationship between large-scale flow pattern, cloud cover, and snowfall is reasonably straight-forward, but does not lead to widespread significant trends in surface variables (Fig. 9). The coverage of the anti-cyclonic warming trend shown by CFSR in Fig. 2a is effectively downscaled by WRF, covering the southeastern part of High Asia and its surroundings at 200 hPa, but excluding the northwestern part (Fig. 9a). Over the area of warming (no warming), there are some negative (positive) trends in 300-hPa cloud ice and snowfall, but there is relatively little area covered by significant trends (Fig. 9b, c). The map of T2m trends does not bear any resemblance to the other trends, however, and just shows some warming along the Himalaya (Fig. 9d). The lack of resemblance between cloud trends and T2m trends is likely because winter temperature is less dependent on cloud cover and is also driven by cold-air and warm-air outbreaks. Because winter temperatures are of little relevance for glacier melt, these temperature trends are not investigated further.

### 5.1.2 Local trends

Cross sections at locations indicated in the top panels of Fig. 9 illustrate the climatology and changes of these winter flow patterns from 1979–1980 to 2014–2015 from the perspective of the Karakoram and CH (Fig. 10, left and right panels, respectively). Over both locations, there is a band of climatological winter cloud ice above 500 hPa (Fig. 10, top panels). Liquid cloud is mostly confined to the first major orographic barrier over the western and central Himalaya, as has been shown for orographic precipitation in general (e.g., Bookhagen and Strecker 2008), due to cross-barrier moisture transport from extratropical cyclones (e.g., Lang and Barros 2004; Barros et al. 2006; Cannon et al. 2015; Norris et al. 2015), but with a secondary maximum over the Karakoram. The magnitudes of cloud ice and liquid cloud are both far greater over the western Himalaya and Karakoram than CH and Tibet, reflecting the greater occurrence of extratropical cyclones further west.

Significant positive (negative) trends in cloud ice are exhibited near the Karakoram (CH), but the glaciers themselves are minimally affected (Fig. 10, second row). There

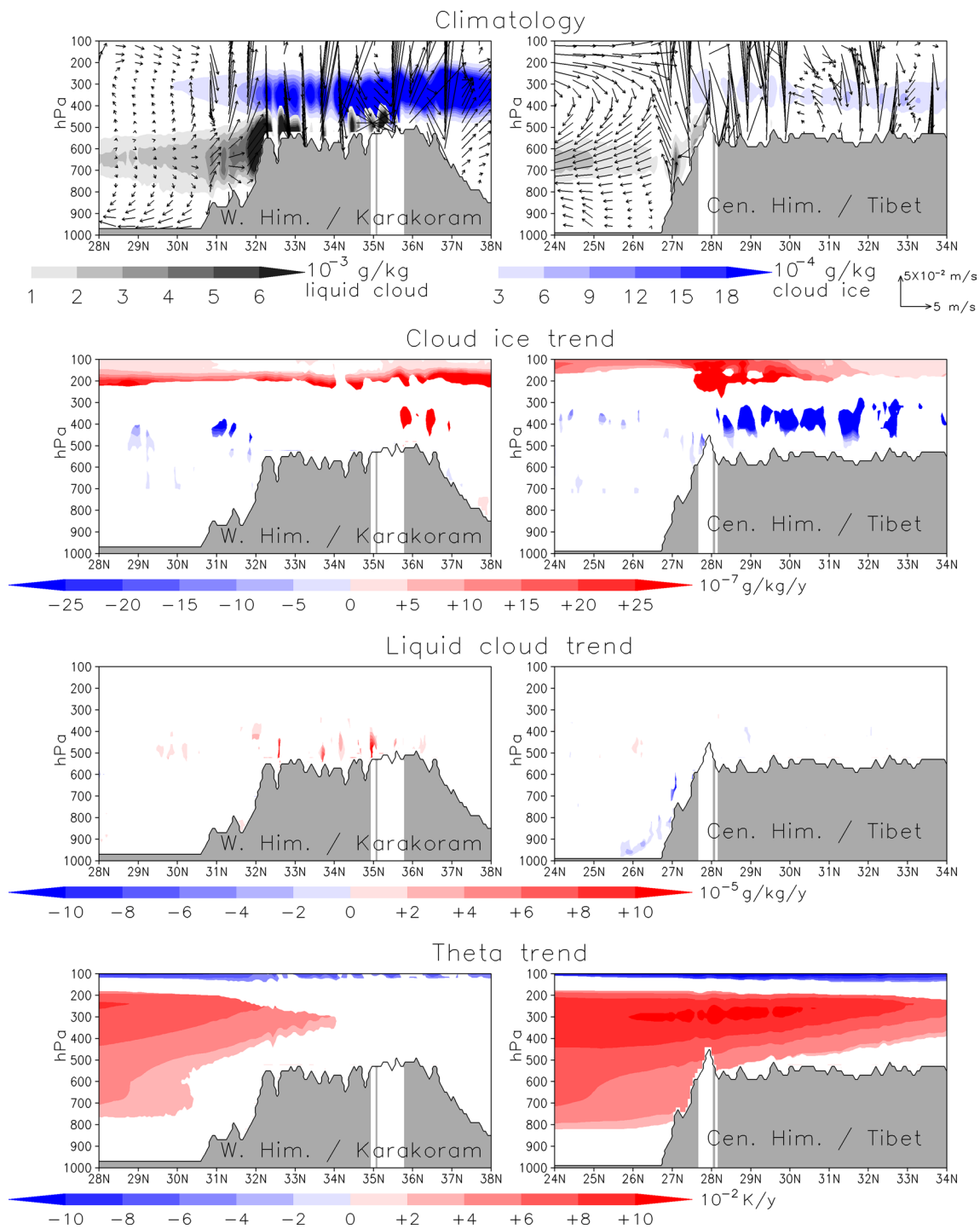


**Fig. 10** Meridional cross sections in DJF from 1979–1980 to 2014–2015 across the the western Himalaya/Karakoram (left panels) and CH/Tibet (right panels) at the locations shown in Fig. 9. Top row shows climatologies of cloud ice (blues), liquid cloud (grays), and

winds ( $v$  and  $w$ , re-scaled according to the relative  $y$  and  $z$  scales of the cross section). Bottom three rows are as Fig. 9 for the indicated variables, but in the lat- $p$  plane. The locations of the Karakoram and CH glaciers are shown in white

are also significant positive trends in liquid cloud near the Karakoram, with no trends over or near the CH (Fig. 10, third row). The lack of surface warming over the Karakoram previously noted is placed in context by the large

gap in the positive potential-temperature,  $\theta$ , trend above the western Himalaya and Karakoram, in contrast to the widespread warming extending to the surface above the CH (Fig. 10, bottom row). These  $\theta$  trends correspond to the

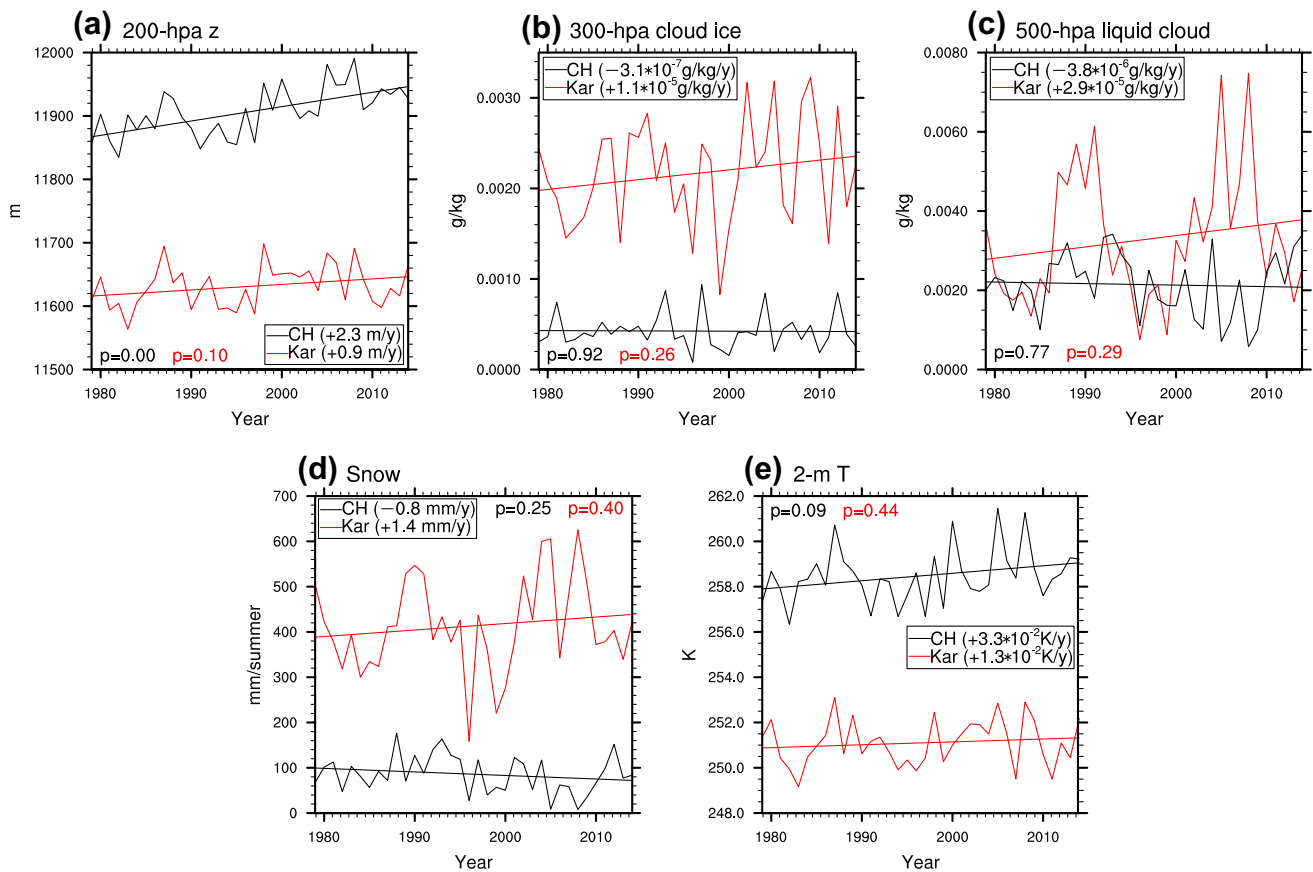


**Fig. 11** Interannual timeseries of the indicated variables throughout the downscaling in DJF. Each entry is calculated from the mean of all glaciated grid points in the CH or Karakoram (locations shown in Fig. 1b), taking the total (snowfall) or mean (other variables) over

upper-tropospheric geopotential-height trends (Fig. 9a) and directly result from the large-scale trends exhibited by the reanalyses. Also exhibited in both cross sections are significant positive trends in cloud ice at about 200 hPa (Fig. 10, second row) and significant cooling at 100 hPa (Fig. 10, bottom row). These are almost certainly due to an expansion of the troposphere with global warming and relatively uniform in horizontal plots (not shown), and so are not considered relevant for glacier mass balance.

Averaged over the CH and Karakoram, there is a highly significant upward trend in 200-hPa geopotential height over the CH but not Karakoram (Fig. 11a), but this has not resulted in significant trends in 300-hPa cloud ice, 500-hPa liquid cloud, or snowfall over either region, although there are upward trends in cloud and snowfall over the Karakoram that are rendered insignificant by large interannual variability (Fig. 11b–d). There are also no significant trends in T2m, averaging over each region, although there is a 1-K increase in the trend from 1979 to 2014 over the CH that is rendered insignificant by large interannual variability (Fig. 11e). Thus, in winter, despite a clear divide between an

winter. The trends of the timeseries are also shown, with their magnitudes (rounded to two significant figures) and significance levels (two decimal places) indicated

anti-cyclonic warming trend in the upper troposphere over the CH and no such trend over the Karakoram, the downscaling does not identify any significant precipitation or 2-m temperature trends.

## 5.2 Summer trends

### 5.2.1 Large-scale trends

In summer, mechanisms explaining snowfall and temperature trends are more complex and result from a combination of effects that, to be properly understood, require more variables at different pressure levels (Fig. 12). As in winter, the anti-cyclonic warming trend shown by CFSR in Fig. 2c is effectively downscaled by WRF, covering the southeastern part of High Asia and its surroundings at 200 hPa, excluding the northwestern part (Fig. 12a). Consequently, at 300 hPa, cloud ice has significantly decreased over most of central and eastern High Asia, with the greatest decreases co-located with the maximum in the geopotential-height trend, whereas the western part containing the Karakoram

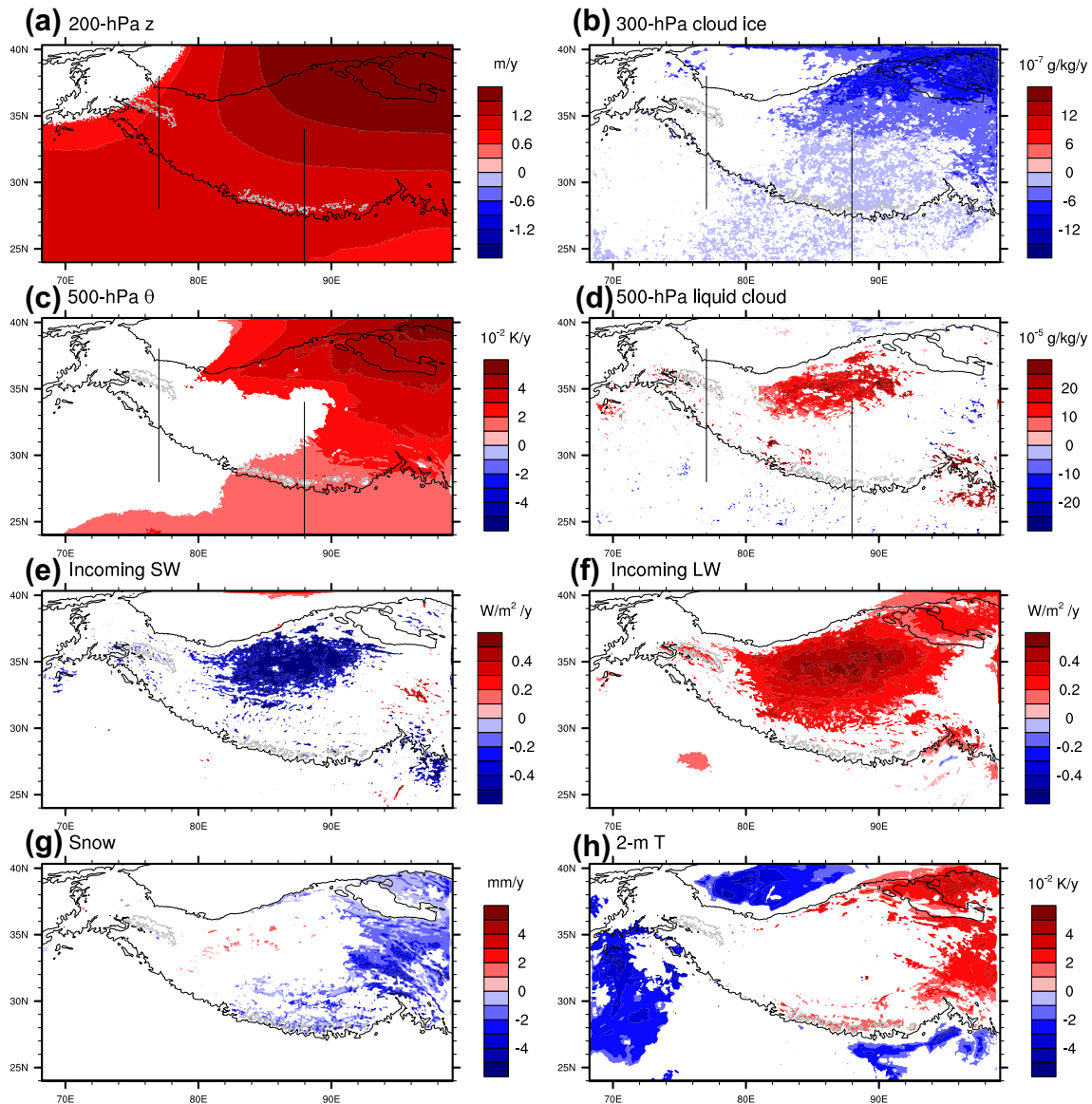


**Fig. 12** As Fig. 9, but for the given variables in JJA from 1979 to 2014. The lines in the panels of pressure-level variables show the locations of the cross sections across the western Himalaya/Karakoram and CH/Tibet in Fig. 13

shows mostly neutral trends (Fig. 12b). At 500 hPa, there is an increasing trend in liquid cloud over the central Tibetan Plateau and parts of western High Asia (Fig. 12d), corresponding to the gap in the positive  $\theta$  trend at the same level (Fig. 12c).

The cloud trends, particularly at 500 hPa, closely resemble those of surface variables (Fig. 12e–h). On the large-scale, positive (negative) cloud trends in Fig. 12b, d are collocated with negative (neutral) trends in incoming shortwave radiation (Fig. 12e), positive (neutral) trends in incoming longwave radiation (Fig. 12f), neutral (negative) trends in snowfall (Fig. 12g), and negative (positive) trends in T2m (Fig. 12h). However, there is no significant trend in T2m

over most of central and western High Asia, suggesting that a decrease in shortwave radiation may have been offset by an increase in longwave radiation. The area of decreasing cloud ice (Fig. 12b), decreasing snowfall (Fig. 12g) and increasing T2m (Fig. 12h) is very similar to that shown by surface-temperature observations over the Tibetan Plateau (Wang et al. 2008; Gao et al. 2015) and precipitation observations from APHRODITE (Malik et al. 2016, based on a quantile regression). With their 30-km multi-decadal WRF down-scaling, Gao et al. (2015) showed that this near-surface warming is associated with a negative trend in lapse rate, consistent with the positive trend in geopotential height over this part of the Tibetan Plateau (Fig. 12a). This area



has therefore experienced increased stability, reduced cloud cover, reduced snowfall, and warming. Contrastingly, the area with increasing liquid cloud (Fig. 12d) and decreasing shortwave radiation (Fig. 12e) is co-located with a gap in the areas of snowfall and temperature changes (Fig. 12g, h), suggesting that the increase in the simulated cloudiness has offset the drying and warming trends over the northern/central Tibetan Plateau associated with the larger-scale anti-cyclonic trend (Fig. 12a). Because the emphasis for this study is on trends over the CH and Karakoram, the trends over Tibet are not further investigated.

It is important to note that surface temperature in summer is not purely determined by cloud cover and responds to a combination of factors, including changes in horizontal advection and increase in subsidence, which may have contributed to surface warming over this area, considering the anti-cyclonic trend. Zhao et al. (2014) related cooling of west Asia and warming of east Asia in summer to differential advection due to the weakening monsoon (see the schematic in their Fig. 10). Furthermore, Forsythe et al. (2015) found that in JJA daily maximum temperature at PMD/WAPDA stations and daytime MODIS cloud cover are correlated between  $-0.1$  and  $-0.7$ , depending on the specific month and station (their Fig. 8a), indicating that summer surface temperature is not solely dependent on cloud cover. However, of relevance to the current study, their figure shows that higher-elevation stations have greater negative correlations, with all correlations  $< 0.4$  and statistically significant for stations above 3 km elevation. Therefore, although surface temperature is not solely dependent on cloud cover, the results of Forsythe et al. (2015), together with the similarity of the areas of negative cloud trends, and positive T2m trends in the current study (Fig. 12) strongly suggest that reduced cloud has played a significant role in daytime surface warming over southeastern High Asia.

### 5.2.2 Local trends

Within the regions of broadly positive or negative trends of the fields shown in Fig. 12 there is considerable spatial variability (Fig. 12—all panels except those showing geopotential height and  $\theta$ ), reflecting how the complex terrain modifies the large-scale trends. Cross sections taken at the locations indicated in Fig. 12 illustrate the climatology and changes of these summer flow patterns from 1979 to 2014 from the perspective of the Karakoram and CH (Fig. 13, left and right panels, respectively), as for winter trends in Fig. 10. Over both locations, there is a band of climatological summer cloud ice between about 300 and 100 hPa (Fig. 13, top panels), indicating the layer of the atmosphere in which cloud ice predominantly forms. The climatology indicates that cloud ice forms sufficiently high in summer to be relatively independent of orography. By contrast, liquid

cloud is mostly confined to the first major orographic barrier in the mid-troposphere, as in winter (Fig. 10, top row), due to moisture advection from the monsoonal flow. This monsoon circulation is exhibited in the top panels of Fig. 13 as a southerly (cross-barrier) jet at low levels, with ascent at the orographic barrier, and northerly returning flow aloft. Near the western Himalaya, however, there are climatological southerlies in the upper troposphere, co-located with the climatological maximum cloud ice.

Over both locations, there is a negative trend in cloud ice from 300 hPa upward (Fig. 13, second row), co-located with warming (Fig. 13, bottom row). This cloud-ice reduction and warming extend to the surface over the CH and there are statistically significant downward wind vectors below areas of cloud-ice reduction, indicating that, when averaged over summer, there has been less ascent forming these clouds, likely due to the anticyclonic trend. Contrastingly, there is no warming and little reduction in cloud ice below 300 hPa over the western Himalaya and Karakoram. This area between 500 and 300 hPa is where the pronounced southerly trend lies over the western Himalaya and Karakoram. This southerly trend is the eastern flank of the cyclonic trend over west Asia and has likely offset the large-scale warming in the upper troposphere. Additionally, there is an increase in liquid cloud on the windward side of the mountains over the western Himalaya and Karakoram at midlevels of the troposphere (roughly between 700 and 500 hPa), with no trend over the CH (Fig. 13, third row).

The contrasting trends between the CH and Karakoram in summer months since 1979 are summarized in Fig. 14. At 200 hPa there is a significant increase in geopotential height over both the CH and Karakoram of similar magnitude (Fig. 14a), but lower down at 500 hPa there is significant warming over the CH but not Karakoram (Fig. 14c). There is a significant decreasing trend in cloud ice over the CH at 300 hPa (and at 500 hPa, not shown), but with no trend in cloud ice over the Karakoram (Fig. 14b). The lack of an increasing liquid-cloud trend at 500 hPa over the CH (Fig. 14d), despite warming, indicates a net decrease in condensate over the CH. By contrast, the significant positive trend in liquid cloud over the Karakoram (Fig. 14d), given that there are no trends in cloud ice, indicates a net increase in condensate over the Karakoram. Consequently, there is a significant decreasing trend in downward shortwave radiation over the Karakoram (Fig. 14e) and a significant increasing trend in downward longwave radiation (Fig. 14f). There is no significant trend in downward shortwave radiation over the CH (Fig. 14e), despite the significantly reduced cloud cover, but this relationship is likely better explained by trends in the diurnal cycle, which are not investigated in this study. Despite the lack of a significant trend in downward shortwave radiation over the CH, the time series of 500-hPa liquid cloud and

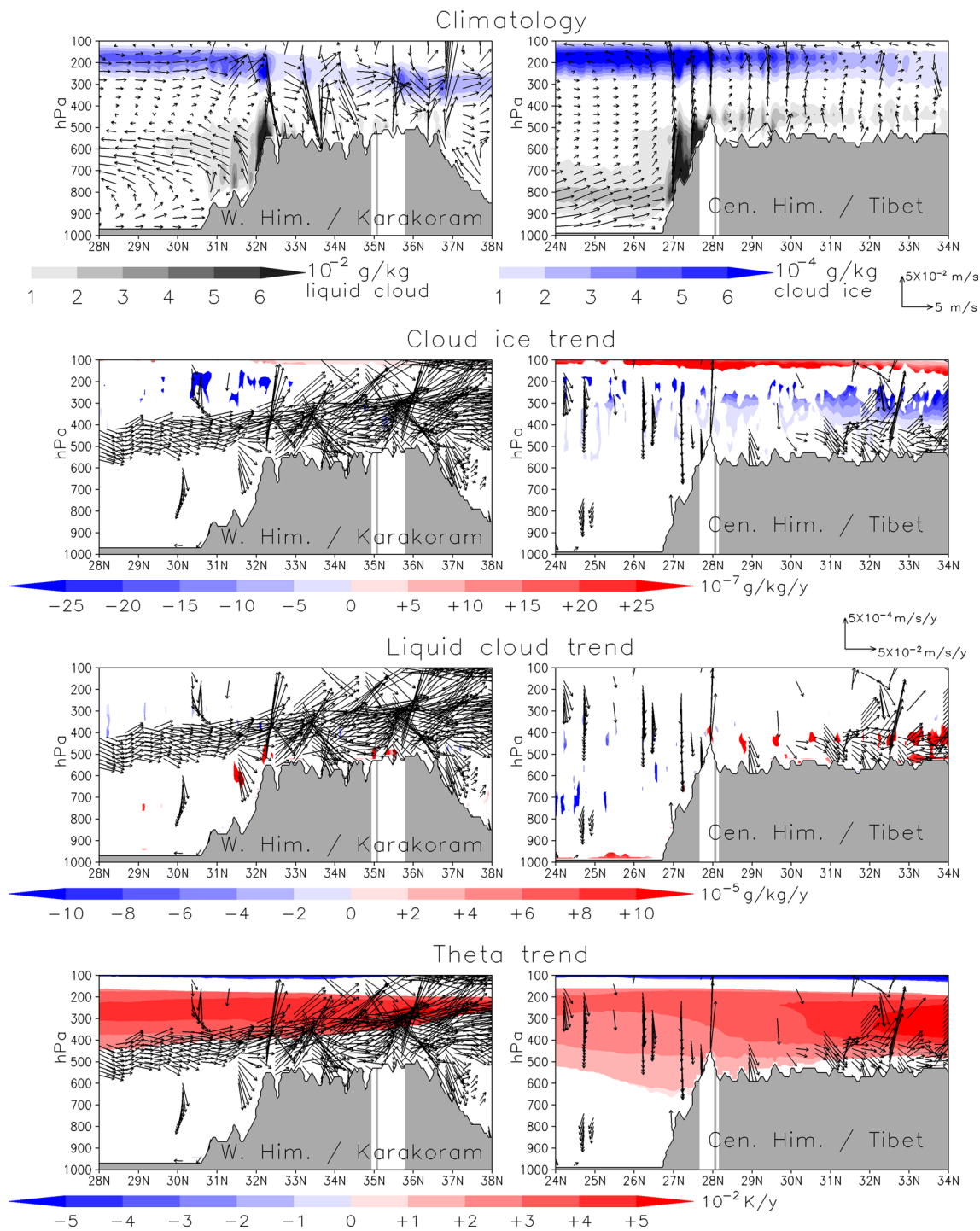


**Fig. 13** As Fig. 10, but for JJA from 1979 to 2014, and also including trends in the  $v$ - $w$  wind vectors (plotted where either the  $v$  or  $w$  trend is significant at the 5% level)

downward shortwave radiation have highly significant ( $p < 0.005$ ) correlations of  $-0.92$  over the CH (and  $-0.83$  over the Karakoram). Therefore, the downscaling shows a strong relationship whereby greater (less) cloud cover implies less (more) incoming shortwave radiation, when averaged over a summer season.

Regarding meteorological forcing of glacier advance/retreat, these cloud and radiation trends mean that over the CH in summer snowfall has significantly decreased by  $1.9$  mm/year (Fig. 14g) and T2m has significantly increased by  $0.014$  K/year (Fig. 14h). Meanwhile, there is no significant trend in snowfall or T2m over the Karakoram (Fig. 14g, h).

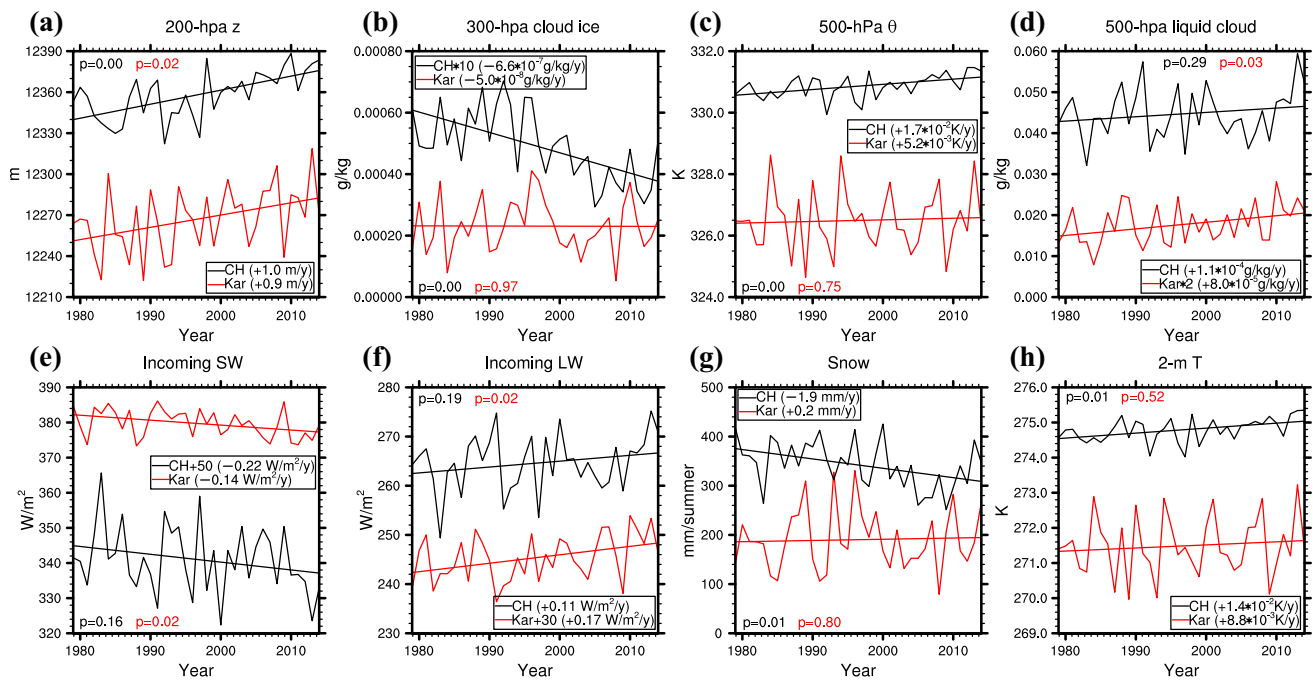


**Fig. 14** As Fig. 11, but for the given variables in JJA. Some timeseries are re-scaled or have a constant added as indicated in order to plot the CH and Karakoram timeseries together. Where timeseries have been

re-scaled, the given value for the trend is of the original timeseries, not the re-scaled timeseries

Therefore, according to the downscaling the increasing liquid cloud over the Karakoram in summer has not resulted in a significant increase in snowfall, and the decreasing short-wave radiation has not resulted in significant cooling.

Although the downscaling captures differences in trend between the CH and Karakoram, particularly in summer, which may explain the contrasting glacier behaviour between these two regions, there are no differences captured between the Karakoram and its closer surrounding mountain ranges. In particular, glaciers in the Hindu Kush and western Himalaya regions have exhibited rapid glacier loss in recent decades (Bolch et al. 2012; Gardelle et al. 2013; Kaab et al. 2015), but the downscaling shows no trends in snowfall or T2m over any glaciated regions within 500 km or so of the Karakoram that are consistent with glacier retreat (bottom row of Figs. 9 and 12). Thus, this downscaling is unable to address the contrast in glacier mass balance between the Karakoram and its immediate neighboring ranges. Performing a higher-resolution downscaling would possibly identify these heterogeneous trends, or it is possible that these contrasts are driven by factors that a purely meteorological model is unable to address. Regardless, the downscaling has identified strongly contrasting snowfall and surface-temperature trends between the Karakoram and CH that may be a significant factor in the observed glacier retreat over the CH but not Karakoram. Further research is required to address

why other glaciers near the Karakoram have not behaved as those on the Karakoram itself.

## 6 Summary and conclusions

Karakoram glaciers have been stable or even advanced, while other glaciers in High Mountain Asia including the central Himalaya have retreated at particularly high rates in recent decades. To investigate snowfall and temperature trends associated with this differential between central Himalayan and Karakoram glaciers, 36 years of CFSR were dynamically downscaled with WRF over High Mountain Asia from 1979–2015. In all four seasons, CFSR exhibits positive trends in geopotential height over most of High Mountain Asia, indicating tropospheric warming. Most relevantly, in winter and summer, the eastern part of High Asia, including the central Himalaya, has been affected by an anti-cyclonic warming trend, whereas the western part of High Asia, including the Karakoram, has been affected by a cyclonic trend with no warming.

In winter, areas of cyclonic (anti-cyclonic) trends are co-located with increasing (decreasing) cloud cover in the upper troposphere and increasing (decreasing) snowfall, but only small areas exhibit significant trends in cloud or snowfall. Trends in 2-m temperature are not similarly distributed, with just significant warming along part of the

Himalaya, but are considered less relevant because even with warming winter temperatures are still well below freezing.

In summer, the most distinctive differences between the central Himalaya and Karakoram are observed. The anti-cyclonic trend over the eastern part of High Asia has reduced cloud cover from the surface upward, including over the central Himalaya. Although there are no significant trends in incoming shortwave radiation, there are significant trends of reduced snowfall and warming over the central Himalaya in summer, likely related to the reduction in cloud cover.

In summer, the Karakoram is near the edge of the anti-cyclonic trend in the upper troposphere, and there is no significant trend in potential temperature near the surface, unlike most of the region that shows a widespread positive trend. The Karakoram shows significant trends of increasing cloud cover and decreasing incoming shortwave radiation. Despite these trends in cloud cover and radiation, there are no significant trends in snowfall or 2-m temperature. The regional trends in summer shown by WRF are consistent with rapid glacier retreat over the central Himalaya and stable/advancing glaciers over the Karakoram.

Although the downscaling identified trends over the central Himalaya consistent with glacier retreat, there are other glaciers nearer the Karakoram (e.g., Hindu Kush and the western Himalaya) where glaciers have also retreated in recent decades (Bolch et al. 2012; Gardelle et al. 2013; Kaab et al. 2015), where this downscaling did not identify any trends to contrast with those over the Karakoram. Additional studies are required to investigate whether higher resolution can identify more localized snowfall or temperature trends. There are some factors relevant to glacier retreat/advance that are not represented by a purely atmospheric model (e.g., debris cover of glaciers and aerosol concentration). A dynamical downscaling should not be considered a complete model for calculating glacier advance/retreat and is likely insufficient to fully explain the Karakoram anomaly. Nevertheless, from a meteorological perspective, the contrasting trends in both winter and summer between the Karakoram and central Himalaya identified by this downscaling may explain a great deal of the observed variability in glacier retreat/advance within the region.

**Acknowledgements** This research was supported by the Climate and Large-scale Dynamics Program, from the National Science Foundation (NSF award-AGS 1116105) and by the U.S. National Aeronautics and Space Administration (NASA) Headquarters under the NASA Earth and Space Science Fellowship Program (Grant no. 13-EARTH13F-26). The CFSR data used in this research were developed by NCEP and provided by NCAR, available at <http://rda.ucar.edu/pub/cfsr.html>. ERA-Interim data were developed by ECMWF and made available through NCAR (<https://rda.ucar.edu/datasets/ds627.2/>). In-situ precipitation and temperature data were provided by PMD and WAPDA. MODIS data were obtained from [http://modis-atmos.gsfc.nasa.gov/MOD06\\_L2](http://modis-atmos.gsfc.nasa.gov/MOD06_L2).

High-performance computing support from Yellowstone (ark:/85065/d7wd3xhc) was provided by NCAR's Computational and Information Systems Laboratory (CISL), sponsored by the NSF. Thanks to the anonymous reviewers whose comments have greatly improved this manuscript.

## References

- Archer DR, Fowler HJ (2004) Spatial and temporal variations in precipitation in the Upper Indus Basin, global teleconnections and hydrological implications. *Hydrol Earth Syst Sci* 8:47–61
- Bao X, Zhang F (2013) Evaluation of NCEP-CFSR, NCEP-NCAR, ERA-Interim, and ERA-40 reanalysis datasets against independent sounding observations over the Tibetan Plateau. *J Clim* 26:206–214
- Barros AP, Lang TJ (2003) Monitoring the monsoon in the Himalayas: observations in central Nepal, June 2001. *Mon Weather Rev* 131:1408–1427
- Barros AP, Chiao S, Lang TJ, Burbank D, Putkonen J (2006) From weather to climate-seasonal and interannual variability of storms and implications for erosion processes in the Himalaya, vol 398. Geological Society of America, Special Paper, Boulder, pp 17–38
- Bolch T, Kulkarni A, Kääb A, Huggel C, Paul F, Cogley JG, Frey H, Kargel JS, Fujita K, Scheel M, Bajracharya S, Stoffel M (2012) The state and fate of Himalayan glaciers. *Science* 336:310–314
- Bollasina M, Bertolani L, Tartari G (2002) Meteorological observations at high altitude in the Khumbu Valley, Nepal Himalayas, 1994–1999. *Bull Glaciol Res* 19:1–11
- Bookhagen B, Strecker MR (2008) Orographic barriers, high-resolution TRMM rainfall, and relief variations along the eastern Andes. *Geophys Res Lett* 35:L06403
- Bookhagen B, Burbank DW (2010) Towards a complete Himalayan hydrological budget: the spatiotemporal distribution of snowmelt and rainfall and their impact on river discharge. *J Geophys Res* 115:F03019
- Cannon F, Carvalho LMV, Jones C, Bookhagen B (2015) Multi-annual variations in winter westerly disturbance activity affecting the Himalaya. *Clim Dyn* 44:441–455
- Cannon F, Carvalho LMV, Jones C, Norris J, Bookhagen B, Kiladis GN (2017) Effects of topographic smoothing on the simulation of winter precipitation in High Mountain Asia. *J Geophys Res Atmos* 122:1456–1474
- Dee DP, Uppala SM, Simmons AJ, Berrisford P, Poli P, Kobayashi S, Andrae U, Balmaseda MA, Balsamo G, Bauer P, Bechtold P, Beljaars ACM, van de Berg L, Bidlot J, Bormann N, Delsol C, Dragani R, Fuentes M, Geer AJ, Haimberger L, Healy SB, Hersbach H, Hólm EV, Isaksen L, Kållberg P, Köhler M, Matricardi M, McNally AP, Monge-Sanz BM, Morcrette J-J, Park B-K, Peubey C, de Rosnay P, Tavolato C, Thépaut J-N, Vitart F (2011) The ERA-Interim reanalysis: configuration and performance of the data assimilation system. *Q J R Meteorol Soc* 137:553–597
- Duan K, Yao T, Thompson LG (2006) Response of monsoon precipitation in the Himalayas to global warming. *J Geophys Res* 111:D19110. <https://doi.org/10.1029/2006JD007084>
- Fowler HJ, Archer DR (2006) Conflicting signals of climate change in the Upper Indus Basin. *J Clim* 19:4276–4293
- Forsythe N, Hardy AJ, Fowler HJ, Blenkinsop S, Kilsby CG, Archer DR, Hashmi MZ (2015) A detailed cloud fraction climatology of the Upper Indus Basin and its implications for near-surface air temperature. *J Clim* 28:3537–3556
- Forsythe N, Fowler HJ, Li X-F, Blenkinsop S, Pritchard D (2017) Karakoram temperature and glacial melt driven by regional atmospheric circulation variability. *Nat Clim Chang* 7:664–670

- Gardelle J, Berthier E, Arnaud Y (2012) Slight mass gain of Karakoram glaciers in the early twenty-first century. *Nat Geosci* 5:322–325
- Gardelle J, Berthier E, Arnaud Y, Kääb A (2013) Region-wide glacier mass balances over the Pamir–Karakoram–Himalaya during 1999–2011. *Cryosphere* 7:1263–1286
- Gao Y, Xu J, Chen D (2015) Evaluation of WRF mesoscale climate simulations over the Tibetan Plateau during 1979–2011. *J Clim* 28:2823–2841
- Hasnain SI (2002) Himalayan glaciers meltdown: impact on South Asian rivers. In: van Lanen HAJ, Demuth S (eds) FRIEND 2002—regional hydrology: bridging the gap between research and practice, vol 274. IAHS Publication, London, pp 417–423
- Hewitt K (2005) The Karakoram anomaly? Glacier expansion and the “elevation effect”, Karakoram Himalaya. *Mt Res Dev* 25:332–340
- Hong S-Y, Noh Y, Dudhia J (2006) A new vertical diffusion package with an explicit treatment of entrainment processes. *Mon Weather Rev* 134:2318–2341
- Houze RA Jr, Wilton DC, Smull BF (2007) Monsoon convection in the Himalayan region as seen by the TRMM precipitation radar. *Q J R Meteorol Soc* 133:1389–1411
- Iacono MJ, Delamere JS, Mlawer EJ, Shephard MW, Cloud SA, Collins WD (2008) Radiative forcing by long-lived greenhouse gases: calculations with the AER radiative transfer models. *J Geophys Res* 113:D13103
- Kääb A, Berthier E, Nuth C, Gardelle J, Arnaud Y (2012) Contrasting patterns of early twenty-first-century glacier mass change in the Himalayas. *Nature* 488:495–498
- Kääb A, Treichler D, Nuth C, Berthier E (2015) Brief communication: contending estimates of 2003–2008 glacier mass balance over the Pamir–Karakoram–Himalaya. *Cryosphere* 9:557–564
- Kain JS (2004) The Kain–Fritsch convective parameterization: an update. *J Appl Meteorol* 43:170–181
- Krishnan R, Sabin TP, Ayantika DC, Kitoh A, Sugi M, Murakami H, Turner AG, Slingo JM, Rajendran K (2013) Will the South Asian monsoon overturning circulation stabilize any further? *Clim Dyn* 40:187–211
- Lang TJ, Barros AP (2004) Winter storms in the Central Himalayas. *J Meteor Soc Jpn* 82:829–844
- Liu C, Ikeda K, Thompson G, Rasmussen RM, Dudhia J (2011) High-resolution simulations of wintertime precipitation in the Colorado Headwaters region: sensitivity to physics parameterizations. *Mon Weather Rev* 139:3533–3553
- Medina S, Houze RA Jr, Kumar A, Niyogi D (2010) Summer monsoon convection in the Himalayan region: terrain and land cover effects. *Q J R Meteorol Soc* 136:593–616
- Malik N, Bookhagen B, Mucha PJ (2016) Spatiotemporal patterns and trends of Indian monsoonal rainfall extremes. *Geophys Res Lett* 43:1710–1717
- Mölg T, Maussion F, Collier E, Chiang JCH, Scherer D (2017) Prominent midlatitude circulation signature in High Asia’s surface climate during monsoon. *J Geophys Res Atmos* 122:12,702–12,712
- Monin AS, Obukhov AM (1954) Basic laws of turbulent mixing in the surface layer of the atmosphere. *Tr Akad Nauk SSSR Geofiz Inst* 24(151):163–187
- Niu G-Y, Yang Z-L, Mitchell KE, Chen F, Ek MB, Barlage M, Kumar A, Manning K, Niyogi D, Rosero E, Tewari M, Xia Y (2011) The community Noah land surface model with multiparameterization options (NoahMP): 1. Model description and evaluation with local scale measurements. *J Geophys Res* 116:D12109
- Norris J, Carvalho LMV, Jones C, Cannon F (2015) WRF simulations of two extreme snowfall events associated with contrasting extratropical cyclones over the western and central Himalaya. *J Geophys Res* 120:3114–3138
- Norris J, Carvalho LMV, Jones C, Cannon F, Bookhagen B, Palazzi E, Tahir AA (2017) The spatiotemporal variability of precipitation over the Himalaya: evaluation of one-year WRF model simulation. *Clim Dyn* 49:2179–2204
- Rango A, Martinec J (1995) Revisiting the degreeday method for snowmelt computations. *Water Resour Bull* 31(4):657–669
- Roxy MK, Ritika K, Terray P, Murtugudde R, Ashok K, Goswami BN (2015) Drying of Indian subcontinent by rapid Indian Ocean warming and a weakening land–sea thermal gradient. *Nat Commun* 6:7423. <https://doi.org/10.1038/ncomms8423>
- Saha S, Moorthi S, Pan H-L, Wu X, Wang J, Nadiga S, Tripp P, Kistler R, Woollen J, Behringer D, Liu H, Stokes D, Grumbine R, Gayno G, Wang J, Hou Y-T, Chuang H-Y, Juang H-MH, Sela J, Iredell M, Treadon R, Kleist D, Van Delst P, Keyser D, Derber J, Ek M, Meng J, Wei H, Yang R, Lord S, van den Dool H, Kumar A, Wang W, Long C, Chelliah M, Xue Y, Huang B, Schemm J-K, Ebisuzaki W, Lin R, Xie P, Chen M, Zhou S, Higgins W, Zou C-Z, Liu Q, Chen Y, Han Y, Cucurull L, Reynolds RW, Rutledge G, Goldberg M (2010) The NCEP climate forecast system reanalysis. *Bull Am Meteorol Soc*. 1015–1057 <https://doi.org/10.1175/2010BAMS3001.1>
- Scherler D, Bookhagen B, Strecker MR (2011) Spatially variable response of Himalayan glaciers to climate change affected by debris cover. *Nat Geosci* 4:156–159
- Shrestha AB, Wake CP, Mayewski PA, Dibb JE (1999) Maximum temperature trends in the Himalaya and its vicinity: an analysis based on temperature records from Nepal for the period 1971–94. *J Clim* 12:2775–2786
- Skamarock WC, Klemp JB, Dudhia J, Gill DO, Barker DM, Duda MG, Huang X-Y, Wang W, Powers JG (2008) A description of the advanced research WRF version 3. NCAR Technical Note NCAR/TN-475+STR. NCAR, Boulder
- Stauffer DR, Seaman NL (1990) Use of four-dimensional data assimilation in a limited-area mesoscale model. Part I: experiments with synoptic-scale data. *Mon Weather Rev* 118:1250–1277
- Stauffer DR, Seaman NL, Binkowski FS (1991) Use of four-dimensional data assimilation in a limited-area mesoscale model. Part II: effects of data assimilation within the planetary boundary layer. *Mon Weather Rev* 119:734–754
- Tahir AA, Chevallier P, Arnaud Y, Ahmad B (2011) Snow cover dynamics and hydrological regime of the Hunza River basin, Karakoram Range, Northern Pakistan. *Hydrol Earth Syst Sci* 15:2275–2290
- Thompson G, Field PR, Rasmussen RM, Hall WD (2008) Explicit forecasts of winter precipitation using an improved bulk microphysics scheme. Part II: implementation of a new snow parameterization. *Mon Weather Rev* 136:5095–5115
- Thompson G, Tewari M, Ikeda K, Tessendorf S, Weeks C, Otkin J, Kong F (2016) Explicitly-coupled cloud physics and radiation parameterizations and subsequent evaluation in WRF high-resolution convective forecasts. *Atmos Res* 168:92–104
- Wang B, Bao Q, Hoskins B, Wu G, Liu Y (2008) Tibetan Plateau warming and precipitation changes in East Asia. *Geophys Res Lett* 35:L14702. <https://doi.org/10.1029/2008GL034330>
- Wang B, Long CN, Leung LR, Dudhia J, McFarlane SA, Mather JH, Ghan SJ, Liu X (2009) Evaluating regional cloud-permitting simulations of the WRF model for the Tropical Warm Pool International Cloud Experiment (TWP-ICE), Darwin, 2006. *J Geophys Res* 114:D21203. <https://doi.org/10.1029/2009JD012729>
- Wilks DS (2006) *Statistical methods in the atmospheric sciences*. Elsevier, Burlington
- Yamada T, Shiraiwa T, Iida H, Kadota T, Watanabe T, Rana B, Ageta Y, Fushimi H (1992) Fluctuations of the glaciers from the 1970s to 1989 in the Khumbu, Shorong and Langtang regions, Nepal Himalayas. *Bull Glacier Res* 10:11–19
- Yasutomi N, Hamada A, Yatagai A (2011) Development of a long-term daily gridded temperature dataset and its application to rain/

- snow discrimination of daily precipitation. *Glob Environ Res* V15N2:165–172
- Yatagai A, Kamiguchi K, Arakawa O, Hamada A, Yasutomi N, Kitoh A (2012) APHRODITE: constructing a long-term daily gridded precipitation dataset for Asia based on a dense network of rain gauges. *Bull Am Meteorol Soc.* <https://doi.org/10.1175/BAMS-D-11-00122.1>
- Zhao Y, Huang A, Zhou Y, Huang D, Yeng Q, Ma Y, Li M, Wei G (2014) Impact of the middle and upper tropospheric cooling over Central Asia on the summer rainfall in the Tarim Basin, China. *J Clim* 27:4721–4732